

1 **Wintertime organic and inorganic aerosols in Lanzhou, China:**
2 **Sources, processes and comparison with the results during**
3 **summer**

4

5 **J. Xu¹, J. Shi², Q. Zhang³, X. Ge⁴, F. Canonaco⁵, A. S. H. Prévôt^{5,6}, M. Vonwiller⁷, S.**
6 **Szidat⁷, J. Ge², J. Ma⁸, Y. An¹, S. Kang¹, D. Qin¹**

7 ¹State Key Laboratory of Cryospheric Sciences, Cold and Arid Regions Environmental
8 and Engineering Research Institute, CAS, Lanzhou 730000, China

9 ²Key Laboratory for Semi-Arid Climate Change of the Ministry of Education, College of
10 Atmospheric Sciences, Lanzhou University, Lanzhou 730000, China

11 ³Department of Environmental Toxicology, University of California, Davis, CA 95616,
12 USA

13 ⁴Jiangsu Key Laboratory of Atmospheric Environment Monitoring and Pollution Control
14 (AEMPC), School of Environmental Science and Engineering, Nanjing University of
15 Information Science & Technology, Nanjing 210044, China

16 ⁵Laboratory of Atmospheric Chemistry, Paul Scherrer Institute (PSI), Villigen 5232,
17 Switzerland

18 ⁶State Key Laboratory of Loess and Quaternary Geology and Key Laboratory of Aerosol
19 Chemistry and Physics, Institute of Earth Environment, Chinese Academy of Sciences,
20 710075 Xi'an, China

21 ⁷Department of Chemistry and Biochemistry & Oeschger Centre for Climate Change
22 Research, University of Bern, Berne, 3012, Switzerland

23 ⁸College of Earth Environmental Science, Lanzhou University, Lanzhou 730000, China

24

25 Correspondence to: J. Xu (jzxu@lzb.ac.cn)

26

27 **Abstract**

28 Lanzhou, which is located in a steep Alpine valley in western China, is one of the most
29 polluted cities in China during the wintertime. In this study, an Aerodyne high resolution
30 time-of-flight aerosol mass spectrometer (HR-ToF-AMS), a seven-wavelength
31 aethalometer, and a scanning mobility particle sizer (SMPS) were deployed during
32 January 10 to February 4, 2014 to study the mass concentrations, chemical processes, and
33 sources of sub-micrometer particulate matter (PM₁). The average PM₁ concentration
34 during this study was 57.3 μg m⁻³ (ranging from 2.1 to 229.7 μg m⁻³ for hourly averages)
35 with organic aerosol (OA) accounting for 51.2%, followed by nitrate (16.5%), sulphate
36 (12.5%), ammonium (10.3%), black carbon (BC, 6.4%), and chloride (3.0%). The mass
37 concentration of PM₁ during winter was more than twice the average value observed at
38 the same site in summer 2012 (24.5 μg m⁻³), but the mass fraction of OA was similar in
39 the two seasons. Nitrate contributed a significantly higher fraction to the PM₁ mass in
40 winter compared to summer (16.5% vs. 10%), largely due to more favoured partitioning
41 to the particle phase at low air temperature. The mass fractions of both OA and nitrate
42 increased by ~5% (47% to 52% for OA and 13% to 18% for nitrate) with the increase of
43 the total PM₁ mass loading, while the average sulphate fraction decreased by 6% (17% to
44 11%), indicating the importance of OA and nitrate for the heavy air pollution events in
45 Lanzhou. The size distributions of OA, nitrate, sulphate, ammonium, and chloride all
46 peaked at ~500 nm with OA being slightly broader, suggesting that aerosol particles were
47 internally mixed during winter, likely due to frequently calm and stagnant air conditions
48 during wintertime in Lanzhou (average wind speed: 0.82 m s⁻¹).

49

50 The average mass spectrum of OA showed a medium oxidation degree (average O/C
51 ratio of 0.28), which was lower than that during summer 2012 (O/C = 0.33). This is
52 consistent with weaker photochemical processing during winter. Positive matrix
53 factorization (PMF) with the multi-linear engine (ME-2) solver identified six OA sources,
54 i.e., a hydrocarbon-like OA (HOA), a biomass burning OA (BBOA), a cooking-emitted

55 OA (COA), a coal combustion OA (CCOA), and two oxygenated OA (OOA) factors.
56 One of the OOAs was less-oxidized (LO-OOA) and the other one of more-oxidized (MO-
57 OOA). LO-OOA was the most abundant OA component (22.3% of OA mass), followed
58 by CCOA (22.0%), COA (20.2%), MO-OOA (14.9%), BBOA (10.8%), and HOA (9.8%).
59 The mass fraction of primary OA (= HOA + BBOA + COA + CCOA) increased during
60 high PM pollution periods, indicating that local primary emissions were a main reason for
61 the formation of air pollution events in Lanzhou during winter. Radiocarbon (^{14}C)
62 measurement was conducted on four $\text{PM}_{2.5}$ filter samples from this study, which allowed
63 for a quantitative source apportionment of organic carbon (OC). The non-fossil sources
64 on average accounted for $55 \pm 3\%$ of OC which could be mainly from biomass burning
65 and cooking activities, suggesting the importance of non-fossil sources for the PM
66 pollution in Lanzhou. Combining with the PMF results, we also found that a large
67 fraction ($66 \pm 10\%$) of the secondary OC was from non-fossil OC.

68

69 **1 Introduction**

70 Frequent haze pollution events in urban areas in China have been a widespread concern
71 in recent years due to its high adverse health effects, visibility degradation and climate
72 effects (Chan and Yao, 2008). The Chinese Central Government had put in extensive
73 efforts to find urgent and suitable control strategies to reduce further deterioration of air
74 quality. Strategies such as promoting energy conservation and emission reduction
75 measures and new air quality standards ($\text{PM}_{2.5}$ currently vs. PM_{10} in the past) have been
76 implemented in the last three years ([http://www.gov.cn/zwggk/2013-
77 09/12/content_2486773.htm](http://www.gov.cn/zwggk/2013-09/12/content_2486773.htm)). Many local governments have also launched measures such
78 as shutting down some highly polluting factories and restricting the use of private
79 vehicles to reduce air pollution in their cities. However, air pollution in China is still far
80 from being controlled due to its complex sources and limited knowledge on the multiple
81 pathways leading to secondary aerosol formation and dynamic variation of aerosol mass
82 loading.

83

84 Lanzhou, the capital of Gansu province, is located at the northwest of China and has
85 experienced air pollution issues since the 1960s due to emissions from the petrochemical
86 industry and its valley terrain which tended to form stagnant meteorological conditions
87 (Tang et al., 1985; Zhang et al., 2000). Air pollution is still serious and has become more
88 variable in recent years (since 2000) because of fast urbanization and increased energy
89 consumption. The severity of air pollution often reaches maximum intensity during
90 winter due to coal combustion for domestic heating and cooking, similar to the situations
91 in most cities of northern China (Wang et al., 2014). Despite the serious air pollution
92 during winter in Lanzhou, aerosol chemistry, sources, and formation and transformation
93 processes were poorly documented in the literature, which limit the development and
94 implementation of efficient control strategies.

95

96 The chemical and physical properties of atmospheric aerosol particles during winter,
97 especially during haze episode, have been recently investigated in metropolitan cities in
98 Eastern China (Sun et al., 2006; Zhao et al., 2013; Huang et al., 2014; Sun et al., 2014).
99 For example, the mean aerosol optical depth at 500 nm were up to ~0.7 during the month-
100 long heavy haze pollution episode during January 2013 in Beijing (Bi et al., 2014); The
101 airborne microbes were found in particulate matter (PM) during hazy period which may
102 potentially include respiratory microbial allergens and pathogens (Cao et al., 2014).
103 Collection and analysis of filter samples have enabled quantification of the chemical
104 composition of PM using a suite of off-line instruments (such as ion chromatography,
105 organic and element carbon analyzer, inductively coupled plasma-mass spectrometry and
106 so on) in the laboratory (He et al., 2001; Zheng et al., 2005; Sun et al., 2006; Sun et al.,
107 2011a; Zhang et al., 2013; Zhao et al., 2013), but often incapable of capturing details of
108 the atmospheric evolution processes during the typical lifecycle of aerosol.

109

110 Previous studies on source apportionment of aerosol particle identified dust, traffic,
111 industry, cooking-related activities, and secondary formation as important contributors,
112 although the contributions of individual sources may change drastically with location,

113 season, and different apportionment algorithms (Zheng et al., 2005; Yu et al., 2013;
114 Huang et al., 2014). For example, Zheng et al. (2005) used chemical mass balance
115 (CMB) receptor model to quantitatively apportion the sources that contribute to fine PM
116 concentration in Beijing and found coal combustion contributed 16% of fine PM mass in
117 January. By contrast, principal component analysis of the same dataset estimated almost
118 twice amount of aerosols from coal combustion (Song et al., 2006). Source
119 apportionment techniques, such as the positive matrix factorization (PMF) allow us to use
120 thousands of fragment ions for source identification and use the real measurement
121 uncertainties to constrain the fitting, and would thus appear more suitable to identify and
122 apportion PM to their sources (Ulbrich et al., 2009). Compared with the number of
123 aerosol source apportionment studies using PMF in Eastern China (e.g., Sun et al., 2013b;
124 Zhang et al., 2013), there were fewer studies in inland cities of China (Elser et al., 2016),
125 the results of which can be used for inter-comparison and understanding the difference of
126 aerosol pollution in different parts of China. In addition, it has been known that a large
127 mass fraction of ambient PM during haze episodes is from fine particles, of which
128 secondary species (some carbonaceous components, sulphate, nitrate, and ammonium)
129 are major components (Zhao et al., 2013). However, the formation and evolution
130 mechanisms of those secondary species were poorly understood, and previous models
131 tended to underestimate the secondary species budget in polluted regions (e.g., Volkamer
132 et al., 2006; Carlton et al., 2010; Hodzic et al., 2016).

133

134 Online instruments based on mass spectrometric techniques, such as Aerodyne aerosol
135 mass spectrometer (AMS) (Jayne et al., 2000), have advantages on probing the fast
136 aerosol chemical processes because of the instrument can output data with a large amount
137 of chemical information and its fine time resolution (in minutes) and mass sensitivity (in
138 ng m^{-3}) (Canagaratna et al., 2007). Aerodyne high resolution time-of-flight mass
139 spectrometer (HR-ToF-AMS) have been widely employed for the chemical
140 characterization of submicron aerosol (PM_{10}) (DeCarlo et al., 2006), which provides on-
141 line quantitative mass spectra of the non-refractory (inorganic and organic) aerosol
142 components with high time resolution. Frequently, the organic aerosol (OA) can be

143 further analyzed using the PMF algorithm (Ulbrich et al., 2009; Zhang et al., 2011a),
144 which can represent the organic mass spectral matrix as a set of source/process-related
145 factor mass spectra and time series. In addition, carbon isotope technique has been
146 recently applied to quantify the fossil/non-fossil origins of carbonaceous aerosols, and in
147 combination with AMS-PMF analyses, the assessment of the origin of secondary organic
148 aerosol (SOA) became possible (Minguillon et al., 2011; Huang et al., 2014; Zotter et al.,
149 2014; Beekmann et al., 2015).

150

151 In a previous study, we used an HR-ToF-AMS to investigate the chemical characteristics
152 of PM₁ in the urban area of Lanzhou during summer 2012 (Xu et al., 2014). During that
153 study, organics in PM₁ was found to mainly originate from traffic, cooking activities, and
154 chemical reactions which produced semi-volatile and less-volatility oxygenated OA.
155 Compared to summer situation, energy consumption for heating is huge during winter
156 and the dry and stable meteorological condition in the valley leads to longer aerosol
157 lifetime during winter. Thus aerosols are influenced largely by very different
158 meteorological conditions and chemical processes between the two seasons. More
159 intensive measurements of PM chemical characteristics are needed to better understand
160 aerosol sources, to quantify their lifetime in the atmosphere and to constrain the
161 uncertainties of their climatic influences. During winter of 2013/2014, we conducted such
162 a study at an urban site of Lanzhou. In this paper, we focus on the chemical speciation of
163 PM₁ and source apportionment of OA.

164

165 **2 Measurement and methods**

166 2.1 Sampling site

167 Aerosol particle measurements were conducted from January 10 to February 4, 2014, at
168 the top floor of a twenty-two story building (~70 m a.g.l) (36.05°N; 103.85°W, 1569 m
169 a.s.l) in the campus of Lanzhou University (Fig. S1a). The campus is located in the
170 Chenguan district of Lanzhou which is a cultural and educational area. The twenty-two
171 story building sits at the western edge of the campus and faces a south-northern arterial

172 road (Fig. S1a). At the campus side of this building, there is a three story dining hall of
173 Lanzhou University, and over the arterial road side, there are many restaurants and
174 residents. The room temperature was kept at ~ 20 °C by a central heating radiator. The
175 weather in Lanzhou during the campaign was cold (avg. $T = 0.5$ °C) and dry (avg. $RH =$
176 28%), and was influenced by the Asian winter monsoon. Because Lanzhou is surrounded
177 by mountains, atmospheric condition is normally stable with low wind speed (on average
178 0.82 m s^{-1} during this study). The sampling site represents a typical urban area dominated
179 by residential and commercial area.

180

181 2.2 Instruments

182 The physiochemical properties of aerosol particles were monitored in real-time by a suite
183 of instruments (Fig. S1b). The sampling inlet, constructed using 0.5 inch copper tube,
184 stemmed out of the rooftop by about 1.5 m. A $PM_{2.5}$ cyclone (model URG-2000-30EH,
185 URG Corp., Chapel Hill, NC, USA) was used for removing coarse particles. The length
186 of the sampling line was about 5 m. A diffusion dryer was placed upstream of this line to
187 eliminate potential RH effect on particles. The inlet was shared by an Aerodyne HR-ToF-
188 AMS (Aerodyne, Inc., Billerica, MA, USA) for the size-resolved chemical speciation of
189 non-refractory sub-micrometer PM ($NR-PM_1$), a single particle intra-cavity laser induced
190 incandescence photometer (SP2, DMT, Inc., Boulder, CO, USA) for refractory black
191 carbon (rBC) measurement, a customer-made scanning mobility particle sizer (SMPS)
192 (Wiedensohler et al., 2012) for measuring particle size distribution between 10-800 nm,
193 and a $7\text{-}\lambda$ aethalometer (model AE31, Magee Scientific, Berkeley, CA, USA) to derive
194 the mass concentration of light absorbing black carbon (BC) particles. The total air flow
195 rate from the inlet was $\sim 16 \text{ L min}^{-1}$, with a vacuum pump drawing the air at a flow rate
196 of 10 L min^{-1} and the other 6 L min^{-1} sampled by the instruments. The retention time of
197 particles in the sampling line was less than 2.5 s. A parallel inlet with a 1:10 dilution
198 stage was setup for real-time $PM_{2.5}$ measurement using a tapered element oscillating
199 microbalance (TEOM series 1400a, R&P, East Greenbush, NY, USA). The roof of the
200 building also hosted instruments for monitoring meteorological parameters such as

201 visibility, air temperature, wind direction, wind speed, and RH. The visibility was
202 measured with a LED-based (880 nm) forward (42°) scattering visibility sensor (model
203 M6000, Belfort Ins., Maryland, USA).

204

205 2.2.1 HR-ToF-AMS operation

206 A detailed description of the principle and design of HR-ToF-AMS can be found
207 elsewhere (Jayne et al., 2000; DeCarlo et al., 2006). Briefly, HR-ToF-AMS consists of
208 three major sections: the inlet system, the particle sizing vacuum chamber, and the
209 particle composition detection section. The combination of a 100 μm orifice and an
210 aerodynamic lens in the inlet system are used to focus the airborne particles into a
211 concentrated and narrow beam, and then accelerated into the vacuum chamber ($\sim 10^5$
212 Torr) modulated by a chopper for measuring aerodynamic size of the particle; Before
213 being detected, the particles are flash vaporized under 600 °C and ionized by a 70 eV
214 electron impact, and finally detected by the high resolution time-of-flight mass
215 spectrometer. The chopper works at three positions alternately, i.e., an open position
216 which transmits the particle beam continuously, a close position which blocks the particle
217 beam completely, and a chopping position which modulates the beam transmission (2%
218 duty cycle). The open and close positions yield the bulk and background signals for the
219 airborne particle, respectively, while the chopping position modulates the particle beam
220 by spinning chopper wheel (~ 150 Hz) to yield size-resolved spectral signals. The mass
221 spectrometer in the detection section works in two modes based on the shape of the ion
222 path, i.e., V-mode and W-mode, with high sensitivity and high resolution (~ 6000 m/ Δ m),
223 respectively. The highly sensitive V-mode signals are usually used for reporting mass
224 concentration, while the high chemical resolution W-mode signals are used for the
225 analyses of mass spectrum. The time resolution for both V and W modes was 5 min.
226 Under V-mode, the instrument switched between the mass spectrum mode and the PToF
227 mode every 15 s, spending 6 and 9 s on each, and cycled 20 times in one run; No PToF
228 data were recorded in W-mode due to low signal-to-noise (S/N) ratios.

229

230 The instrument was calibrated for ionization efficiency (IE), inlet flow rate, and particle
231 sizes using the standard procedure described by (Jayne et al., 2000). For example, the size
232 calibration was performed following the general protocol used in the AMS community.
233 We used standard polystyrene latex (PSL) spheres (Duke Scientific Corp., Palo Alto, CA)
234 (100-700nm) and mono-dispersed ammonium nitrate particles (100-300nm), respectively.
235 These three calibrations were performed at the beginning, in the middle and end of the
236 field study. Particle-free ambient air was sampled at the end of the study to determine the
237 detection limits (DLs) of individual species and also for adjusting the fragmentation
238 table. Note that since no in-situ measurement of gas phase CO₂, the subtraction of a
239 constant CO₂ signal (400 ppm based on filtered-air measurement in this study) may
240 introduce uncertainties in the quantification of the organic-CO₂⁺ signal. However, this
241 artifact was expected to be small (less than 5% error in organic-CO₂⁺ quantification) due
242 to the high OA concentration (Xu et al., 2014). Default relative ionization efficiency
243 (RIE) values were assumed for organics (1.4), nitrate (1.1), sulphate (1.2), and chloride
244 (1.3), while an RIE value of 3.9 was determined for ammonium following the analysis of
245 pure NH₄NO₃. The close concentrations between measured ammonium and predicted
246 ammonium based on the stoichiometric charge balance between nitrate, sulphate, and
247 chloride (slope = 0.94, Fig. S4) suggest that these RIE values are suitable for this
248 campaign.

249

250 2.2.2 Operations of other instruments

251 The SMPS consisting of a condensation particle counter (CPC) (TSI, model 3772) and a
252 differential mobility analyser (DMA) was deployed at 5 min interval. Sample and sheath
253 flow rates of the DMA were set to 1 L min⁻¹ and 5 L min⁻¹, respectively. The SMPS was
254 calibrated using a polystyrene latex (PSL) standard prior to field measurements.

255

256 The SP2 uses an intra-cavity Nd:YAG laser at 1064 nm to determine the light scattering
257 and laser-induced incandescence of individual rBC (namely material associated with a
258 strongly absorbing component at 1064 nm). The SP2 incandescence signal was used to

259 obtain single particle rBC mass after calibration with Aquadag standard BC particles. The
260 measured rBC mass is converted to a mass equivalent diameter, which is termed as the
261 BC core diameter (D_c) - the diameter of a sphere containing the same mass of rBC as
262 measured in the particle. Any measured particle with a detectable incandescence signal is
263 referred to as an rBC particle, whereas a particle which only exhibits a scattering signal is
264 termed as a non-BC particle. The total rBC mass loading is reported as the sum of all
265 detected single particle rBC masses.

266

267 The aethalometer measures the optical attenuation (absorbance) of light from LED lamps
268 emitting at seven wavelengths (370, 470, 520, 590, 660, 880, and 950 nm) with a typical
269 half-width of 20 nm. The difference in light transmission through the particle-laden
270 sample spot and a particle free reference spot of the filter is attributed to the absorption
271 caused by aerosol. The attenuation of light is converted to the BC mass concentration
272 using wavelength-dependent calibration factors as recommended by the manufacturer.
273 BC was measured using data at 880 nm using a specific attenuation cross section of 16.6
274 $\text{m}^2 \text{g}^{-1}$ during the campaign. The flow rate was maintained at 4.8 L min^{-1} calibrated using
275 a flow meter. Detection limit of the aethalometer BC was determined to be 0.16–0.28 μg
276 m^{-3} with a flow rate of 4.8 LPM and 5 min time interval, calculated as three times the
277 standard deviation (3σ) of the dynamic blanks. The TEOM was operated at a temperature
278 of 40 °C other than normal operation condition (50 °C) to dry the aerosol in order to
279 minimize mass loss due to volatilization of semi-volatile aerosol compounds. The time
280 resolution of $\text{PM}_{2.5}$ mass concentration was 5 min.

281

282 2.3 Data processing

283 2.3.1 General AMS data processing

284 The HR-ToF-AMS data were processed using the standard software of SQUIRREL
285 (v1.56) and PIKA (v1.15c) ([http://cires.colorado.edu/jimenez-](http://cires.colorado.edu/jimenez-group/ToFAMSResources/ToFSoftware/index.html)
286 [group/ToFAMSResources/ToFSoftware/index.html](http://cires.colorado.edu/jimenez-group/ToFAMSResources/ToFSoftware/index.html)) to determine the mass
287 concentrations and the size distributions of the NR- PM_1 species and the ion-specified

288 mass spectra of organics, written in IGOR (Wavemetrics, Inc., Lake Oswego, OR, USA).
289 An empirical particle collection efficiency (CE) of 0.5 was used, which has been widely
290 used in field studies employing AMS with a dryer installed in front of the equipment's
291 particle inlet. This CE value was further validated by the consistency and reasonable
292 slope between HR-ToF-AMS measured mass concentrations and SMPS-determined
293 particle volumes (section 3.1.2, $R^2 = 0.9$, slope = 1.48). The elemental ratios of OA (O:C,
294 H:C, and OM:OC) for this study was determined using the "Aiken ambient" method
295 (Aiken et al., 2008) other than the "improved-ambient" method (Canagaratna et al., 2015)
296 which increased O:C on average by 27%, H:C on average by 10%, and OM:OC on
297 average by 7% (Fig. S2). These "Aiken ambient" results of elemental ratios are more
298 suitable here to allow for comparison with those during summer 2012. In addition, the
299 concentration of PAH was generated in SQUIRREL panel based on the default
300 fragmentation table (Dzepina et al., 2007).

301

302 2.3.2 Positive Matrix Factorization (PMF) analyses

303 The source decomposition of organics was analysed by PMF with the multilinear engine
304 (ME-2) algorithm which serves to reduce rotational ambiguity within the PMF2
305 algorithm. The ME-2 algorithm allows the user to add a priori information into the model
306 (e.g., source profiles) to constrain the matrix rotation and separate the mixed solution or
307 the weak solution. The PMF analysis of organic matrix using ME-2 algorithm is
308 implemented within the toolkit SoFi (Source Finder) and perform by the so-called a-value
309 approach (Canonaco et al., 2013). First, organic matrix was analysed using the PMF2.exe
310 algorithm in robust mode (Paatero and Tapper, 1994) and explored using the PMF
311 Evaluation Toolkit (PET) (Ulbrich et al., 2009). The PMF solution was evaluated
312 following the procedures outlined in Table 1 of Zhang et al. (2011a) including
313 modification of the error matrix and downweight of low S/N ions. Moreover, based on
314 the AMS fragmentation table, some organic ions were not directly measured but scaled to
315 the organic signal at m/z 44, which were downweighted by increasing their errors by a
316 factor of 3. The results of four, five, and six factor solutions with f_{Peak} at 0 are shown in

317 supplementary material (Fig. S5-S7). It is easy to find that a coal combustion-emitted OA
318 (CCOA) factor, a cooking-emitted OA (COA) factor, a less-oxidized and more-oxidized
319 OA (LO-OOA and MO-OOA) factors could be clearly separated in the four-factor
320 solution; for the CCOA factor, there were significant contributions from m/z 55, 57, 60,
321 73, 91, and 115 in the mass spectrum, suggesting a mixing of multiple sources. In the
322 five-factor solution, a hydrocarbon-like OA (HOA) factor was separated; however, m/z
323 60 and 73 which are related to biomass burning OA (BBOA) could not be separated. We
324 then performed OA source apportionment using the ME-2 algorithm by constraining the
325 profiles of HOA and BBOA with the fixed α -value of 0.1 for HOA and 0.4 for BBOA.
326 The α -value test was performed following the technical guidelines presented in Crippa et
327 al. (2014). The reference profile of HOA was adopted from the HOA of the summer
328 study and the reference profile of BBOA was adopted from the nine-factor PMF solution
329 of this study.

330

331 The size distributions of individual OA factors were determined via a multivariate linear
332 regression technique (Ge et al., 2012). This algorithm assumes that each OA mass
333 spectrum is the linear superposition of the mass spectra of individual OA factors, whose
334 mass profiles are constant across the whole size range. Further details about the algorithm
335 can be found in Xu et al. (2014).

336

337 2.3.3 Radiocarbon (^{14}C) data analysis

338 In order to identify the origins of SOA, we conducted ^{14}C analysis on four filter samples.
339 These filter samples were collected at the CAEERI site which is about 500 m away from
340 the LZU site (Fig. S1a). Filter samples were collected using a low volume $\text{PM}_{2.5}$ sampler
341 (16.7 L min^{-1}) during January 2014 with a 24 h sampling time in every week for each
342 filter (January 3rd, 8th, 15th, and 23rd, respectively) on pre-baked quartz filters. One
343 field blank filter was collected and analysed to correct the filter sample measurements.
344 Here, we use the results of these four filter samples to roughly represent the average
345 situation of the field sampling because of the relative stable meteorological conditions

346 (section 3.1.1) and similar aerosol sources during the field study (section 3.1.3). Due to
 347 the limitation of the small amount of filter samples, the results based on this carbon
 348 isotopic data are preliminary and comprehensive validation is an ongoing work. Organic
 349 carbon (OC) was separated from the filters by combustion at 375 °C during 200s in pure
 350 oxygen in a thermo-optical OC/EC analyser (Model 4L, Sunset Laboratory Inc, USA)
 351 (Zhang et al., 2012). The carbon isotopic analysis was conducted by online coupling of
 352 the OC/EC analyser with the accelerator mass spectrometry system MICADAS at the
 353 University of Bern, Switzerland (Zotter et al., 2014; Agrios et al., 2015). Fossil ¹⁴C
 354 measurement results were transferred into the non-fossil fraction (f_{NF}) of OC using a
 355 conversion factor of 1.03 (Zhang et al., 2015b).

356

357 For the apportionment of AMS-PMF OA factors using ¹⁴C data (Zotter et al., 2014), we
 358 assume that all OC sources are represented by the six PMF factors and the f_{NF} in NR-PM₁
 359 was the same as that in PM_{2.5}. The OA mass of each PMF factor and total OA were first
 360 converted to OC mass using the OM:OC ratios derived from its MS (OM:OC_{HOA} = 1.29,
 361 OM:OC_{BBOA} = 1.5, OM:OC_{COA} = 1.27, OM:OC_{CCOA} = 1.37, OM:OC_{LO-OOA} = 1.55,
 362 OM:OC_{MO-OOA} = 2.01, OM:OC_{total} = 1.51). For the OC mass concentration of the AMS
 363 factors, the following notations, hydrocarbon-like organic carbon (HOC), biomass
 364 burning organic carbon (BBOC), cooking organic carbon (COC), coal combustion
 365 organic carbon (CCOC), oxygenated organic carbon (OOC), total organic carbon from
 366 AMS (TOC_{AMS}), were adopted in the following sections. An f_{NF} value was assumed a
 367 priori for the primary PMF factors HOC, BBOC, COC, and CCOC. The average f_{NF} of
 368 OOC is then derived by the equation below:

369

$$370 \quad f_{NF_OOC} = (TOC_{NF_AMS} - f_{NF_HOC} \times HOC - f_{NF_BBOC} \times BBOC - f_{NF_COC} \times COC - f_{NF_CCOC} \\ 371 \quad \times CCOC) / (SV-OOC + LV-OOC)$$

372 Here HOC is assumed to originate from gasoline and diesel exhaust and contains
 373 exclusively of fossil carbon, i.e., $f_{NF_HOC} = 0$; BBOC is estimated to be originated from
 374 biomass burning, i.e., $f_{NF_BBOC} = 1$; COC is assumed to originate from non-fossil carbon

375 such as cooking oil and dressing, i.e., $f_{NF_COC} = 1$; CCOC is estimated to originate from
376 coal combustion, i.e., $f_{NF_CCOC} = 0$.

377

378 **3 Results and discussions**

379 3.1 Overview of field study

380 3.1.1 Meteorological conditions

381 Fig. 1 shows the time series of meteorological parameters and PM_{10} components during
382 the campaign. The measurement site mainly received air masses from northern and
383 northeastern associated with low wind speeds (WS) ranging from 0.6 to 1.1 $m\ s^{-1}$ (on
384 daily average: $0.8 \pm 0.2\ m\ s^{-1}$). The mountains to the north and south of the city could
385 significantly reduce the wind speeds. Air temperature ranged from -5.0 to $6.6\ ^\circ C$
386 (average = $0.6 \pm 3.9\ ^\circ C$) for the diurnal variation during the campaign, but had an evident
387 increase after the Chinese New Year (January 31, 2014) (Fig. 1a). No precipitation event
388 occurred during the campaign, and RH was pretty low ranging from 16.8 to 39.5% (on
389 daily average = $27.5 \pm 7.4\%$) for the diurnal variation. Overall, the meteorological
390 conditions during the campaign were much stable and dryer than those during summer
391 2012 (on average: $1.2 \pm 0.6\ m\ s^{-1}$ for WS and $60 \pm 17\ %$ for RH).

392

393 3.1.2 Inter-comparisons

394 The inter-comparisons between AMS *vs.* SMPS and TEOM are shown in Fig. S3.
395 Comparison between the mass concentration of PM_{10} and the volume of particle measured
396 by SMPS is tightly correlated ($R^2 = 0.9$) with a slope of 1.48, which represents the
397 average density of bulk particles, assuming that the AMS and the SMPS measure a
398 similar particle population. This value is indeed very close to the estimated PM_{10} density
399 (1.46) based on the measured particle composition for this study (using density of $1.2\ g\ m^{-3}$
400 m^{-3} for organics, $1.72\ g\ m^{-3}$ for NH_4NO_3 , $1.77\ g\ m^{-3}$ for $(NH_4)_2SO_4$, $1.52\ g\ m^{-3}$ for NH_4Cl
401 and $1.8\ g\ m^{-3}$ for BC) (Zhang et al., 2005; Bond and Bergstrom, 2006). The mass
402 concentration of PM_{10} is also closely correlated ($R^2 = 0.71$) with TEOM $PM_{2.5}$

403 concentrations with a slope of 0.73. Similar contribution of PM₁ to PM_{2.5} were also
404 observed in other cities in China during winter (Elser et al., 2016), such as Beijing (0.74
405 during 2011) (Sun et al., 2013b). Note that the actual mass ratio between PM₁ and PM_{2.5}
406 should be higher than these values since refractory materials such as crustal components
407 were not measured.

408

409 3.1.3 PM₁ composition, variation, and acidity

410 The average mass concentration of PM₁ (NR-PM₁ + BC) was 57.3 μg m⁻³ (ranging from
411 2.1 to 229.7 μg m⁻³ for hourly average) during this study, with 51.2% of organics, 16.5%
412 of nitrate, 12.5% of sulphate, 10.3% of ammonium, 6.4% of BC, and 3.0% of chloride
413 (Fig. 2a). The average mass concentration was more than twice the average value
414 observed during summer 2012 (24.5 μg m⁻³). All species showed similar day-to-day
415 variation with nitrate being the most significant one (Fig. 1e), suggesting an important
416 local source for nitrate. The mass contributions of PM₁ species from low to high PM₁
417 concentrations showed an increased contribution for organics (49% to 53%) and nitrate
418 (13% to 18%), but a decreased contribution for sulphate (17% to 11%) and BC (7.3% to
419 5.3%) suggesting somewhat different chemical processes/sources for each species during
420 the haze pollution (Fig. 2b). Specifically, the increased organics was mainly due to the
421 contribution of primary OA (POA) based on PMF analysis (more discussion are given in
422 section 3.5). During the late part of Chinese New Year holiday (February 3 to end of the
423 study), PM₁ concentration decreased in association with increased wind speed (~1 m s⁻¹
424 to 2 m s⁻¹). NR-PM₁ appeared to be neutralized throughout this study, as indicated by an
425 overall stoichiometric charge balance between the anions (i.e., nitrate, sulphate, and
426 chloride) and the cation ammonium (slope = 0.94, Fig. S4). This result indicates that the
427 inorganic particulate species were mainly present in the forms of NH₄NO₃, (NH₄)₂SO₄,
428 and NH₄Cl in PM₁.

429

430 3.1.4 Size distribution

431 The average chemically-resolved size distributions of NR-PM₁ species are shown in Fig.
432 3a. While all components peaked between 400–500 nm, organic aerosol presented a
433 wider distribution than the inorganics and extended to ~250 nm, suggesting the influence
434 of fresh organics (POA, more discussion are given in section 3.4). These features were
435 similar to those found in most urban sites by the AMS. The similar mode size of
436 inorganics and SOA (Fig. 3c) suggested the well internally mixed air mass during the
437 sampling period. The mass contributions of chemicals at the major peak (400–500 nm)
438 were organics (~50%), nitrate (~20%), ammonium (~15%), sulphate (~10%), and
439 chloride (~5%); while the contribution of organics increased with the decreasing of size
440 mode (Fig. 3c). Comparing with the results observed during 2012 summer, the size
441 distributions of aerosol particle during winter were narrower, although the mode sizes of
442 major peaks were similar, indicating highly mixed and aged aerosol particles during
443 winter. Note that chloride also showed a wider distribution which was more similar with
444 organics other than sulphate and nitrate. This was not observed during 2012 summer and
445 could be related with OA emitted from coal combustion and biomass burning during
446 wintertime. Note that chloride also showed a wider distribution which was more similar
447 with organics other than sulphate and nitrate. This was not observed during 2012 summer
448 and could be related with OA emitted from coal combustion and biomass burning during
449 wintertime.

450

451 3.2 Diurnal variations of aerosol species

452 All species show significant diurnal variations during the study suggesting the important
453 local and regional sources of aerosol (Fig. 4). The observed diurnal trends of BC
454 presented two dominant peaks with one at late morning (10:00–12:00) and another at
455 early evening (20:00–22:00). The morning peak did not overlap with the rush hours
456 (7:00–9:00), different than that of summer 2012; the BC mass loading started to increase
457 from 6:00 continuously during morning, and reached maximum between 10:00–12:00
458 and then dropped down after the noon time. Another combustion tracer, carbon monoxide

459 (CO), also showed the similar morning peak (Fig. 5). This morning peak was likely
460 resulted from the contribution of multiple combustion sources, such as coal combustion,
461 biomass burning, and traffic emission which had different morning peaks (see section
462 3.4), and the formation of inversion layer during winter at Lanzhou which promoted
463 accumulation of air pollutants from enhanced human activities in the morning. This
464 inversion layer frequently formed from night time and diffused after the noon time due to
465 the valley terrain (Zhang et al., 2011b). The temperature profile observed at the suburban
466 Lanzhou (Yuzhong, ~30 km from the sampling site) showed a strong inversion in the low
467 boundary layer during the morning time (Fig. S8). But such influences should be further
468 verified in the future with simultaneous measurements from boundary layer heights. The
469 evening peak of BC could result from increased human activities such as traffic, cooking,
470 and heating coupled with low boundary layer after sunset. Organics had two sharp peaks
471 at the noon time (12:00–13:00) and early evening (19:00–20:00) which correspond to
472 lunch time and dinner time, respectively, indicating the importance of cooking-related
473 emissions of OA. PMF analysis show that cooking-emitted aerosol could contribute up to
474 50% of organics during meal times (section 3.4.3).

475

476 Sulphate presented two peaks with one occurring at the noon time (11:00–14:00) in
477 accordance with the photochemical processes; this peak is narrower than that during
478 summer, likely due to relatively weak photochemical activities. Another minor peak
479 occurred between 20:00–22:00 which was likely due to the lowered boundary layer depth.
480 The significantly higher concentration of sulphate during winter than summer could
481 result from a higher amount of precursor SO₂ emission, wintertime hydroxyl radical
482 formation, and the increased aerosol particle surface due to high PM loadings that
483 facilitated the heterogenous conversion of SO₂ to sulphate (Yong et al., 2012; Pusede et
484 al., 2015; Zheng et al., 2015). The diurnal pattern of sulphate during winter was similar to
485 that of summer 2012 at Lanzhou and summer 2011 at Beijing, but was different from that
486 of Beijing during winter 2011/2012 where aqueous processing was found to could play
487 an important role (Sun et al., 2013b). Chloride had similar diurnal pattern with sulphate,
488 although the evening peak was more obvious. The major source of hydrochloric acid is

489 biomass burning, coal combustion and waste combustion (Ianniello et al., 2011). The
490 significant evening peak could be related with these sources coupled with the shallow
491 boundary layer. The high background concentrations of chloride during day and night
492 suggest a persistent emission of hydrochloric acid which could be from the heating
493 factory and power plants. The diurnal pattern of chloride during winter was different
494 from that during summer 2012 which peaked during the night time due to temperature-
495 dependent gas-particle partitioning. Nitrate peaked between 12:00–16:00, right after the
496 peak of sulphate. The formation of nitrate during afternoon suggests that nitrate was
497 dominated by the homogeneous photochemical production. Fig. 5 shows the variations of
498 NO_x and O_3 calculated from data downloaded from one station monitored by the Ministry
499 of Environmental Protection of China (MEP), ~3 km southwest of sampling site (Fig.
500 S1a); NO had a morning peak (7:00–10:00) and an evening peak (19:00–21:00)
501 corresponding to rush hours; NO_2 increased from 10:00 which formed from NO
502 consumed by O_3 and slightly decreased from 14:00 to 18:00 corresponding to the
503 photolysis of NO_2 and the formation of nitric acid during afternoon. Note that during
504 night time the diurnal variation of O_3 still showed a background (~10 ppb) although the
505 concentrations of NO were up to 50 ppb. This inconsistent was likely due to the
506 instrument drift in the MEP station during long-term observation, however it seemed that
507 the pattern and the amplitude of the diurnal variation of O_3 were reasonable. The diurnal
508 change of NO_x (ΔNO_x) mixing ratio was ~50 ppbv (from 150 to 100 ppbv), while the
509 diurnal change of the sum of ΔO_3 and ΔNO_3^- was ~30 ppbv. Considering the higher
510 mixing layer height during afternoon, it seems that nitrate was mainly formed from the
511 photochemical processing of NO_x . The diurnal pattern of nitrate during winter was vastly
512 different from that during 2012 summer which was mainly controlled by the dynamic of
513 mixing layer and gas-particle partitioning.

514

515 3.3 Bulk characteristics and elemental ratios of OA

516 Table 1 shows the average elemental mass composition and mass contributions of six ion
517 categories to the total organics. Carbon contributed 67% to the organics following by

518 oxygen (23%), hydrogen (9%), and nitrogen (1%); correspondingly, $C_xH_y^+$ dominated the
519 organics by 59%, following by $C_xH_yO_1^+$ (26%), $C_xH_yO_2^+$ (10%), $H_yO_1^+$ (2%), and
520 $C_xH_yN_p^+$ (2%). Compared with the results of 2012 summer, the organics in winter had
521 higher carbon (67% *vs.* 59%) and $C_xH_y^+$ content (59% *vs.* 56%), and lower oxygen
522 content (23% *vs.* 26%) (Fig. 6c); this suggests that the organics during winter had a
523 higher fraction of primary compounds than those during summer which was likely due to
524 weaker photochemical activities, lower boundary layer height and more emissions from
525 primary sources. The average O/C of organics, an indicator for oxidation state, was 0.28
526 during this study which was somewhat lower than that of summer 2012 (0.33) (Fig. 6a
527 and b). Photochemical processing of organics during winter appeared to be significantly
528 weaker and shorter than those during summer as shown by the smaller diurnal peak of
529 O/C (Fig. 6d). In addition, an offset was existed for the O/C diurnal variation between the
530 2012 and 2014 studies especially for night time, which suggested that
531 background/residual aerosol in the summer were more oxidized than in the winter. The
532 diurnal profile of H/C was inversely correlated with that of O/C, and the peaking of
533 organic aerosol concentration usually corresponded to the high H/C ratio and low O/C
534 ratio, indicating the dominant role of primary OA.

535

536 3.4 Source apportionment of OA

537 Source apportionment via PMF with ME2 engine on OA mass spectra resolved six
538 components, i.e., HOA, COA, CCOA, BBOA, LO-OOA, and MO-OOA. Each
539 component has a unique mass spectral pattern, diurnal pattern, and temporary variation
540 which correlated with corresponding tracers such as inorganic species. Two OOA
541 components can be regarded as surrogates of SOA, with MO-OOA for more aged SOA
542 and LO-OOA for fresher SOA; The HOA, BBOA, COA and CCOA components are
543 regarded as POA based on their low O/C ratios and good correlations with primary
544 aerosol tracers (Fig. 7). Comparison with the source apportionment results of summer
545 2012, the organic sources and chemical processes during winter 2013/2014 were more

546 complex due to the multiple primary sources. Detailed discussion of each factor is given
547 in the following subsections.

548

549 3.4.1 HOA

550 HOA factors had been frequently separated from the OA in urban area due to the
551 emission from traffic and/or other fossil combustion activities (e.g., Sun et al., 2011b; Ge
552 et al., 2012). The diurnal pattern of HOA in winter 2013/2014 of Lanzhou shows two
553 predominant peaks in the morning (6:00–10:00) and evening (20:00–21:00), respectively
554 (Fig. 5). The peaks were mainly associated with the traffic rush hours and low PBL depth
555 before and after sunset. The relatively low concentration during afternoon was probably
556 due to the high PBL depth as shown by the mass concentration variations of BC. The
557 correlation between HOA and BC was high ($R^2 = 0.64$, Fig. 7f and Table 2), as a big
558 fraction of BC has been thought to emit from traffic activities. The minimum of HOA
559 concentration, which typically occurred during afternoon or middle night, was still up to
560 $\sim 2 \mu\text{g m}^{-3}$ suggesting a high background of HOA which is likely due to the stagnant air
561 condition unfavourable for the diffusion of aerosol. The size distribution of HOA showed
562 a mode size of $\sim 200 \text{ nm}$ (Fig. 3b) corresponding to the primary emitted aerosol
563 behaviours and HOA could account for $\sim 25\%$ mass of aerosols between 100-300nm (Fig.
564 3c). The average concentration of HOA during 2013/2014 winter was $2.9 \mu\text{g m}^{-3}$
565 accounting for 9.8% of organics (Fig. 8a). This concentration was higher than that of
566 2012 summer in Lanzhou ($2.9 \text{ vs. } 1.8 \mu\text{g m}^{-3}$) likely due to the lower PBL during winter
567 and stagnant air conditions. The mass contribution from HOA is similar to the result of
568 2013 winter at Beijing (9%) which was also the lowest contributor to the total OA (Sun et
569 al., 2013b; Zhang et al., 2014), probably due to more modern vehicles were used in the
570 recent years.

571

572 3.4.2 BBOA

573 BBOA component had been widely observed in USA and European countries during
574 winter due to the traditional wood burning for residential heating (Alfarra et al., 2007).
575 The BBOA component is thought to be less important in China because coal is the major
576 fuel during winter. BBOA could be an important component in China during some
577 special periods. For example, Zhang et al. (2015a) identified a BBOA factor in urban
578 Nanjing, southeast of China, during harvest seasons of summer and autumn because of
579 the burning of straw. The BBOA component has also been identified in some regions in
580 China where the coal resource is scarce. For example, Du et al. (2015) separated a BBOA
581 factor at a rural site of the northern Tibetan Plateau due to the widely usage of cow dung
582 cake for heating in this region. The BBOA component has also been identified during
583 winter in cities in southern China because of rich wood resource in these regions (He et
584 al., 2011; Huang et al., 2011; Huang et al., 2013). To our knowledge, only three recently
585 papers have reported the identification of a BBOA factor during winter using online
586 measurement in an urban area of northern China (Elser et al., 2016; Hu et al., 2016; Sun
587 et al., 2016). Although the high contribution of non-fossil carbonaceous aerosol was
588 found (Zhang et al., 2015b) and the mass spectra of organic in other cities (such as
589 Beijing) during winter have also significant contributions from m/z 60 and 73 (Sun et al.,
590 2013b; Zhang et al., 2014), it is difficult to separate the BBOA using general PMF
591 because of its similar temporal variation with CCOA, such as diurnal pattern (Fig. 4).
592 BBOA contributions presented a clear periodic change (Fig. 1), and on average were high
593 during night time and low during daytime (Fig. 5). This trend is consistent with
594 conventional usage of biomass for heating. The time series of BBOA was also closely
595 correlated with BC and chloride (Table 2) due to significant emission of these species
596 from biomass burning. The average mass concentration of BBOA was $3.2 \mu\text{g m}^{-3}$, on
597 average contributing 10.8% of the total OA mass for the entire study (Fig. 8a), but could
598 reach up to $\sim 20\%$ during night and down to less than 5% during afternoon (Fig. 8b). This
599 average concentration was close to the results observed at southern Chinese cities such as
600 Jiaxing ($\sim 3.9 \mu\text{g m}^{-3}$) (Huang et al., 2013), Kaiping ($\sim 1.36 \mu\text{g m}^{-3}$) (Huang et al., 2011)
601 and Shenzhen ($\sim 5.2 \mu\text{g m}^{-3}$) (He et al., 2011).

602

603 The size distribution of BBOA peaked at ~400nm which is close to accumulation mode
604 (Fig. 3b). This feature could be due to internal mixing or coagulation of particles. The
605 O/C ratio of BBOA is 0.24, which is consistent with the primary BBOA feature (Ortega
606 et al., 2013). The similar O/C and the dominance of an accumulation mode in the size
607 distribution of BBOA were also observed during winter in Fresno, a major city in the
608 Central Valley of California, USA (Ge et al., 2012; Young et al., 2015).

609

610 3.4.3 COA

611 The COA component has been widely identified in urban AMS studies and observational
612 results by other instruments recently, and it is regarded as important source of OA in
613 urban areas (Abdullahi et al., 2013 and references therein). The MS of COA in this study
614 had a major contribution from $C_xH_y^+$ ions (81.6%) with also an important contribution
615 from $C_xH_yO_1^+$ ions (14.7%), similar as those in HOA (81.0% and 13.0%) (Fig. S9). In
616 comparison with the HOA spectrum, COA had a higher m/z 55 to 57 ratio (2.0 vs. 0.8)
617 (Fig. 7) which had been postulated as a significant indicator for COA (Sun et al., 2011b;
618 Mohr et al., 2012). In the V-shape plot defined by Mohr et al. (2012), which uses f_{55} vs.
619 f_{57} after subtracting the contributions from factors of OOA, CCOA, and BBOA (denoted
620 as OOA_CCOA_BBOA_sub, i.e. $f_{55}^{OOA_CCOA_BBOA_sub}$ and $f_{57}^{OOA_CCOA_BBOA_sub}$), the
621 data can be clearly represented with ones during morning close to HOA line and ones
622 during meal times close to COA line (Fig. S10). The MS of COA is highly similar to that
623 of summer 2012 observation ($R^2 = 0.76$, slope = 0.99, Fig. S11) which was found to
624 resemble closely the COA MS from other locations (Xu et al., 2014). In fact, the COA
625 components were found to be associated with heating of cooking oils rather than burning
626 of meat/food itself, and indeed the COA mass spectra from cooking of different dishes
627 were highly similar (He et al., 2010). The O/C and H/C ratios of COA were 0.07 and 1.73,
628 respectively, suggesting its feature as POA. This O/C ratio was slightly lower (0.07 vs.
629 0.11) and the H/C was slightly higher than that of 2012 summer (1.73 vs. 1.69). The size
630 distribution of COA was also peaking between 100–200 nm similar to that of HOA (Fig.

631 3b). The diurnal variation of COA displayed two predominant peaks standing out at lunch
632 time (12:00–13:00) and dinner time (19:00–20:00), respectively (Fig. 5), and a small
633 breakfast peak (~8:00). This pattern was consistent with that of summer 2012 (Fig. 4)
634 which resulted from the consistent routine life during winter and summer. The enhanced
635 COA concentration at dinner time might be mainly due to the low PBL height and the
636 activity of a formal meal with more attendants and longer time than that of lunch. The
637 temporal variation correlated tightly with $C_6H_{10}O^+$ ($R^2 = 0.96$, Fig. 7d) which has been
638 reported as the high resolution mass spectral markers for ambient COA (Sun et al., 2011b;
639 Ge et al., 2012).

640

641 The average contribution of COA to organics was 20.2% (~10–50%) (Fig. 8a) with an
642 average mass concentration of $5.92 \mu\text{g m}^{-3}$ which was much higher than those of HOA
643 and BBOA. This contribution is similar to those in Beijing during winter (average 19% of
644 OA with a range of 16–30%) (Sun et al., 2013b), Fresno (~19% of OA) (Ge et al., 2012),
645 Barcelona (17% of OA) (Mohr et al., 2012), and Paris (11–17%) (Crippa et al., 2013).
646 This high fraction indicates that COA is an important local source of OA in Lanzhou
647 regardless of clear or hazy periods (section 3.5).

648

649 3.4.4 CCOA

650 A CCOA component had been identified in this study with its MS similar to the OA from
651 coal burning in lab study (Dall'Osto et al., 2013). The MS of CCOA had high signals at
652 m/z 41, 43, 44, 55, 57, 69, 91 and 115 (dominated by $C_xH_y^+$ ions) (Fig. 7i) (Elser et al.,
653 2016). $C_xH_y^+$ ions in total account for 69.9% of CCOA MS, following by $C_xH_yO_1^+$
654 (19.2%) and $C_xH_yO_2^+$ (7.1%). The fractions of $C_xH_y^+$ and $C_xH_yO_1^+$ were similar with
655 those in HOA MS (Fig. S9), but the CCOA MS had high signal intensity at m/z 44
656 (mainly CO_2^+) which is different from that of HOA (Fig. 7). This high CO_2^+ fraction was
657 also observed in CCOA MS in Changdao island in China during winter (Hu et al., 2013).
658 Wang et al. (2015) suggested this high CO_2^+ signal is from the oxidative transformation
659 of the pyrolysis products during coal burning. Zhang et al. (2008) reported that 48–68%

660 of particulate organic matter from coal combustion aerosol is found in the form of
661 organic acids. The O/C ratio is thus higher than that of HOA (0.20 vs. 0.10) with a lower
662 H/C ratio (1.54 vs. 1.86). The CCOA also locates in a lower left position in the triangle
663 plot defined by Ng et al. (2010) (Fig. 9a). These features indicate CCOA is a POA factor
664 but is a little more oxygenated than HOA. The time-dependent concentrations of CCOA
665 correlated with BC ($R^2 = 0.59$) and chloride ($R^2 = 0.49$) which also correlated well with
666 HOA and BBOA (Table 2). Note that although the similar temporal variations between
667 BBOA and CCOA, the significant differences between their MS (in particular, m/z 91)
668 suggested their different origins. In addition, high PAH signals had been observed in the
669 CCOA MS (Sun et al., 2016), and this is consistent with previous results that the coal
670 combustion could be a dominate source of PAHs in China (Okuda et al., 2006). The
671 CCOA mass loading remained high from 20:00 to 10:00, slowly decreased to a minimum
672 at 16:00, and then increased from 16:00 to 20:00 (Fig. 5). This diurnal pattern was similar
673 to that of BBOA which were all mainly emitted from heating. The slower decreasing rate
674 during morning and increasing rate during late afternoon for CCOA than those of BBOA
675 could related with wide usage of coal, such as cooking and power plants. In our summer
676 2012 observation, we also observed OA signals from coal combustion which suggest
677 persistent emitted during the whole year in Lanzhou. The size distribution of CCOA
678 peaked ~ 450 nm (Fig. 3b), similar with that of BBOA.

679

680 The average CCOA mass concentration was $6.4 \mu\text{g m}^{-3}$, accounting for 22.0% of total
681 OA mass (Fig. 8a). The mass fraction of CCOA could reach to $\sim 30\%$ of OA during night
682 and decreased to 3% during afternoon (Fig. 8b). This indicates that CCOA was an
683 important OA component similar as that in Beijing OA (15–55%) (Zhang et al., 2014;
684 Elser et al., 2016), but its mass fraction of $\text{PM}_{2.5}$ ($\sim 9\%$) was at the low end of the values
685 observed at Beijing and Xi'an (9–21%) (Huang et al., 2014).

686

687 3.4.5 LO-OOA and MO-OOA

688 Two or more OOA components are commonly separated by PMF in urban areas which
689 correspond to fresh SOA and aged SOA (Jimenez et al., 2009), and the MS of SOA
690 factors all have predominant contributions at m/z 43 and 44. The MS of fresher SOA such
691 as LO-OOA has higher contribution at m/z 43 (mainly $C_2H_3O^+$, accounting for 74% of
692 m/z 43 in this study), while aged SOA such as MO-OOA has higher signal at m/z 44
693 (mainly CO_2^+ , accounting for 99% of m/z 44 in this study). The contribution of $C_xH_yO_1^+$
694 in LO-OOA was 36.8% followed by $C_xH_y^+$ (48.0%), $C_xH_yO_2^+$ (10.3%), $H_yO_1^+$ (1.6%),
695 $C_xH_yN_p^+$ (2.8%), and $C_xH_yO_zN_p^+$ (0.5%) (Fig. S9). The O/C ratio of LO-OOA was 0.33
696 and H/C was 1.47 consistent with fresh SOA. The MS of MO-OOA was comprised of
697 25.3% of $C_xH_yO_2^+$, 35.7% of $C_xH_yO_1^+$, 30.1% of $C_xH_y^+$, 6.7% of $H_xO_1^+$, 1.8% of $C_xH_yN_p^+$,
698 and 0.4% of $C_xH_yO_zN_p^+$ (Fig. S9). The O/C and H/C ratios of MO-OOA were 0.80 and
699 1.14, respectively. These results indicate that the atmospheric oxidation capacity during
700 winter was still somewhat strong. The positions of LO-OOA and MO-OOA in triangle
701 plot of fCO_2^+ vs. $fC_2H_3O^+$ are situated in the space of triangle plot with MO-OOA at the
702 upper left corner (Fig. 9b) and LO-OOA at the lower right space, respectively, suggesting
703 the different oxidation degree of OOA factors. The MS of LO-OOA and MO-OOA were
704 similar with those of summer 2012 ($R^2 = 0.95$ for MO-OOA and $R^2 = 0.80$ for LO-OOA,
705 Fig. S11). Note that the $C_xH_y^+$ ions in LO-OOA were mainly from by m/z 39, 41, 91 and
706 115 (Fig. 7h), which were also found to be enriched in coal combustion organic aerosols.
707 This feature is similar to that of summer 2012, potentially suggesting that part of LO-
708 OOA was from further oxidation of CCOA.

709

710 The temporal variations of LO-OOA and MO-OOA were highly correlated with
711 secondary inorganic species: LO-OOA vs. sulphate ($R^2 = 0.71$) and MO-OOA vs. nitrate
712 ($R^2 = 0.71$) (Fig. 7a and b, Table 2). These patterns are somewhat contradictory to
713 previous AMS findings that LO-OOA typically correlates better with nitrate due to their
714 similar semi-volatile characteristics while MO-OOA tends to correlate better with
715 sulphate as they are both low-volatility species. These correlations were indeed observed

716 during the summer study of 2012 (Xu et al., 2014). The behaviours of the two OOA
717 factors during this study were likely due to the low air temperature and low RH
718 conditions which favoured nitrate formation primarily through photochemical reactions.
719 This phenomenon was also observed in winter time of Beijing (Sun et al., 2013b).

720

721 The diurnal variation profiles of LO-OOA and MO-OOA all showed one bump with the
722 LO-OOA peaking between 11:00–14:00 and MO-OOA peaking between 12:00–18:00,
723 suggesting the importance of photochemical processes for both OOA factors. The size
724 distribution of the OOA (LO-OOA + MO-OOA) had a mode size of ~550 nm (Fig. 3b)
725 reflecting the feature as SOA. This size mode is slightly bigger than those of OOA in
726 other studies such as Fresno (460 nm) and Lanzhou summer 2012 (~450 nm) likely due
727 to the high concentration of gas precursors and longer lifecycle of aerosol during winter.

728

729 The mass concentrations of LO-OOA and MO-OOA were 6.5 and 4.4 $\mu\text{g m}^{-3}$ with the
730 mass contributions of 22.3% and 14.9% to OA, respectively (Fig. 8a). These
731 contributions were lower than those during summer 2012 in Lanzhou (27% for LO-OOA
732 and 32% for MO-OOA) especially for MO-OOA, likely due to the relative weak solar
733 radiation during winter and more primary sources in winter. The diurnal total
734 contribution of OOA (LO-OOA + MO-OOA) varied between 20%–60% (Fig. 8b),
735 suggesting the importance of SOA in the air pollution throughout the day at Lanzhou.

736

737 3.5 Primary and secondary OA

738 As shown in Fig. 2b, the mass fraction of organics increased with the increase of PM_{10}
739 concentration, so it is important to know the relative contributions of primary and
740 secondary OA components during the pollution periods. Fig. 10a shows the scatter plot of
741 SOA (= LO-OOA + MO-OOA) and POA (= HOA + BBOA + COA + CCOA) during this
742 study. Overall, the SOA and POA correlate weakly but when POA concentrations were
743 less than $\sim 15 \mu\text{g m}^{-3}$ and the OA/ PM_{10} mass fractions were less than 0.5 (data points with

744 green/blue colors), they have relative tight correlation ($R^2 = 0.2$). When POA
745 concentrations and Org/PM₁ fractions were large, POA and SOA show almost no
746 correlation, indicating the importance of POA in the severe aerosol pollutions in Lanzhou
747 during winter. This is different than the observation from summer 2012, during which
748 SOA had a stable contribution to PM₁ (Fig. 10b), due to more complex POA sources and
749 larger contributions from these sources to PM₁ mass loading during winter compared to
750 summer. This is even more evident when comparing each POA factor with OA (Fig. 11).
751 The COA had the biggest contribution to the increased organics can explained 51% of the
752 increase of organics, followed by CCOA (19%). The components of HOA and BBOA
753 also had positive contributions to the increase of PM₁ mass. However, both OOA
754 components had negative slopes with organics with LO-OOA being the major one. The
755 phenomenon of POA dominating during haze periods is different from the results in other
756 cities in China (Huang et al., 2014). For example, Elser et al. (2016) found significant
757 increased contribution from SOA and secondary inorganic aerosol during haze periods in
758 2013/2014 winter in Xi'an and Beijing. This is likely due to the higher RH values in the
759 eastern China which is more favourable for the aqueous-phase production of SOA.
760 Indeed, Sun et al. (2013a) observed significant increase of secondary inorganic aerosol
761 during high RH periods in Beijing.

762

763 The average contribution of POA to organics decreased from 63.0% to 39.3% during
764 Chinese New Year festival of 2014 (Fig. 1) due to the reduced primary aerosol sources
765 (many restaurants were closed during the holiday of Chinese New Year) such as HOA
766 (9.8% to 3.3%), COA (20.2% to 11.6%), CCOA (22.0% to 15.4%), and BBOA (10.8% to
767 9.0%). This is an indication that control of cooking activities and traffic emissions in this
768 residential area may be effective strategies for air quality improvement during winter.

769

770 3.6 Fossil and non-fossil OC

771 OC measured by OC/EC analyser on two filters (OC_{filter}) and corresponding AMS
772 (OC_{AMS}) online measured results are shown in Fig. 12a. The average ratio of

773 OC_{AMS}/OC_{filter} was ~ 1.5 for these two filters although the smaller size cut for AMS than
774 filter sampler (PM_{1} vs. $PM_{2.5}$). The possible reasons were likely due to the analytical
775 uncertainties of different instruments (30% for AMS and 20% for OC_{filter}), which was
776 also observed in other studies (Zotter et al., 2014), and negative artifacts for the filter
777 samples. The data from the ^{14}C measurement for the filter samples are listed in Table S1.
778 The total average of f_{NF} in these four filters was $55 \pm 3\%$, with 54% and 57% for filters
779 during Jan. 15 and Jan. 23, respectively. Comparison with other studies, the average f_{NF}
780 value in this study was lower than those in Xi'an (63%) and Guangzhou (65%), and
781 higher than those in Beijing (42%), while similar with those in Shanghai (51%) during
782 2012/2013 winter (Zhang et al., 2015b). Combining with the f_{NF} value (the total average
783 of f_{NF} for the total average AMS results) and the contributions of fossil (F) POC (HOC
784 and CCOC) and non-fossil (NF) POC (BBOC and COC), the f_F and f_{NF} for SOC could be
785 obtained (Fig. 12b). The average f_F and f_{NF} for POC and SOC are summarized into Fig.
786 13. The f_F and f_{NF} for POC during Jan. 15 were 50% and 50%, while for SOC were 32%
787 and 68%. The f_F and f_{NF} for POC during Jan. 23 were 37% and 63%, while for SOC were
788 56% and 44%. For all AMS data, the f_F and f_{NF} in POC were 50% and 50%, while for
789 SOC were $34 \pm 10\%$ and $66 \pm 10\%$. The F-POC during Jan. 15 and Jan. 23 were
790 comprised by 15% and 16% HOC and 35% and 21% CCOC, respectively, and NF-POC
791 by 18% and 13% BBOC and 32% and 50% COC, respectively. For all AMS data, the F-
792 POC was comprised by 17% HOC and 33% CCOC, and NF-POC by 16% BBOC and
793 34% COC.

794

795 3.7 Evolution of OA and relationship between odd oxygen and SOA

796 The evolution of OA chemical composition upon aging has been an important subject
797 which is used to understand the formation of SOA. The methods to characterize this
798 evolution include the application of several specific diagrams, such as the AMS triangle
799 plot (f_{44} vs. f_{43} or $f_{CO_2^+}$ vs. $f_{C_2H_3O^+}$) (Ng et al., 2010) and Van Krevelent plot (H:C vs.
800 O:C) (Heald et al., 2010). In the plot of f_{44} vs. f_{43} of this study (Fig. 9a), the data
801 distributed in a narrow space and move up vertically in the triangle space suggesting

802 significant increasing in f_{44} . The data from the low (night time) to the high (afternoon
803 time) f_{44} value corresponded to the evolution of the photo radiation intensity suggesting
804 the photochemical processes. In the plot of $f_{\text{CO}_2^+}$ vs. $f_{\text{C}_2\text{H}_3\text{O}^+}$ (Fig. 9b), most of data
805 moved out of triangle space because of the high contribution of C_3H_7^+ at m/z 43,
806 especially for data during night time. $f_{\text{CO}_2^+}$ and $f_{\text{C}_2\text{H}_3\text{O}^+}$ both increased before the noon
807 time, after that $f_{\text{C}_2\text{H}_3\text{O}^+}$ stopped at ~ 0.06 and $f_{\text{CO}_2^+}$ kept increase likely suggesting the
808 evolution of LO-OOA to MO-OOA. In comparison to the results in summer 2012, the
809 data in winter were more concentrated in the triangle space suggesting air masses with
810 similar source contribution during winter. The winter data in the Van Krevelen diagram
811 follows a slope of -0.8 (Fig. 14a) which suggest that SOA formation chemistry was a
812 combination of carboxylic acid and alcohol/peroxide formation (-1 to -0.5). This slope is
813 higher than that observed at Changdao (-0.6 , rural site) in China during winter
814 suggesting the less oxidation state of our data.

815

816 In order to understand the possible sources of oxygenated OA, we also compared the
817 diurnal variations between MO-OOA and O_x (Fig. 14b). Both O_x and OOA are products
818 of photochemical reactions and the comparison between O_x and OOA can offer insight
819 into the formation of OA due to the dependence of the ratio on the VOC species
820 (Herndon et al., 2008), assuming aqueous processing and night time oxidation for OOA
821 were less important, such as during this study due to the low RH. High SOA vs. O_x slopes
822 were observed (larger than $0.12 \mu\text{g m}^{-3} \text{ppb}^{-1}$) where aromatic VOC dominated the
823 photochemical processing, while a low slopes ($\sim 0.03 \mu\text{g m}^{-3} \text{ppb}^{-1}$) were observed where
824 alkene VOCs dominated the photochemical processing (Wood et al., 2010; Hayes et al.,
825 2013). Fig. 14b shows the scatter plot between O_x and MO-OOA and sized by the mass
826 concentration of BBOA. O_x and MO-OOA showed tight correlation ($R^2 = 0.95$) with a
827 slope of $0.11 \mu\text{g m}^{-3} \text{ppb}^{-1}$. This result is similar with that found in Beijing during
828 wintertime, which has suggested that semivolatile VOCs (e.g., PAHs) could be the
829 primary precursor of OOA (Hu et al., 2016). Several studies suggested that aromatic
830 VOC is dominant among VOCs in northern China (Zhang et al., 2015c) and can be
831 important contribution for SOA production (Liu et al. 2012). We also did correlation

832 between LO-OOA and Ox, and found the different synchronization of LO-OOA and Ox
833 (Fig. S12). It seems LO-OOA varied two to three hours earlier than Ox, likely suggesting
834 other origination for LO-OOA such as down mixing of mixing-layer aerosol, which is a
835 popular phenomenon in the mountain-valley city (Chen et al., 2009).

836

837 **4 Conclusions**

838 In order to understand the sources and chemical processes of the air pollution during
839 winter in Lanzhou, a field study was conducted at an urban site of Lanzhou during
840 January 10 – February 4, 2014 using a suit of on-line instruments. The results show that
841 the average mass concentration of PM₁ (NR-PM₁ + BC) was 57.3 μg m⁻³ (ranging from
842 2.1 to 229.7 μg m⁻³ for hourly averages), with 51.2% of organics, 16.5% of nitrate,
843 12.5% of sulphate, 10.3% of ammonium, 6.4% of BC, and 3.0% of chloride. This mass
844 concentration was about two times higher than that during summer 2012 in Lanzhou,
845 however, the mass loading levels and chemical compositions were similar to those
846 observed in Beijing during winter. The mass concentration of nitrate and organics
847 increased with the increase of PM₁ loading, while sulphate decreased, indicating the
848 importance of OA and nitrate during severe air pollution. The size distributions of all the
849 species displayed a moderate size at 400–500 nm, suggesting that aerosol particles were
850 largely internally mixed during winter. All species presented significant diurnal
851 variations. BC had two peaks at 10:00–12:00 and 20:00–22:00, respectively. Further
852 analysis indicated that the first peak was resulted from the contribution of multiple
853 combustion sources and could be related with the variations of the boundary layer heights
854 during morning which accumulated the air pollutants from early morning and until the
855 break-up at around noon time (such influences should be further verified in the future
856 with simultaneous measurements from boundary layer heights). The evening peak of BC
857 was related to human activities such as traffic and coal combustion coupled with the
858 shallow PBL. OA presented two peaks corresponding to lunch and dinner time
859 suggesting cooking to be an important source. Sulphate peaked during the noon time
860 (11:00–14:00) indicating the importance of photochemical processes. Nitrate presented

861 an afternoon peak (12:00–16:00) which indicate the photochemical processing of NO_x.
862 The diurnal pattern of nitrate during winter time was significant different from that
863 during summer 2012 which was thought mainly from the mixing down of aloft residual
864 layer. PMF analysis of organic mass spectrum with the ME-2 engine identified six
865 organic aerosol sources: i.e., HOA, BBOA, COA, CCOA, LO-OOA, and MO-OOA.
866 POA, which includes HOA, BBOA, COA, and CCOA, accounted for 63% of OA mass
867 and showed an increased in concentration with the increase of PM₁ loading. This is an
868 indication that POA emission was one of the main reasons for the occurrence of heavy air
869 pollution episodes. The temporal profile of MO-OOA tightly correlated with that of
870 nitrate, while those of LO-OOA with sulphate correlated. This observation was different
871 than those observed during other studies and during summer at Lanzhou, indicating the
872 importance of photochemistry for nitrate during winter in Lanzhou due to cold air
873 temperature and low RH conditions. ¹⁴C analysis of OOC indicated that 60 ± 10% of the
874 SOC was formed from non-fossil source.

875

876 **Acknowledgements**

877 The authors thank their colleagues for continuing support and discussion. This research
878 was supported by grants from the Chinese Academy of Sciences Hundred Talents
879 Program, the Key Laboratory of Cryospheric Sciences Scientific Research Foundation
880 (SKLCS-ZZ-2015-01), the National Natural Science Foundation of China Science Fund
881 for Creative Research Groups (41121001, 21407079, 91544220), and the Chinese
882 Academy of Sciences Key Research Program (KJZD-EW-G03).

883 **References**

884

885 Abdullahi, K. L., Delgado-Saborit, J. M., and Harrison, R. M.: Emissions and indoor
886 concentrations of particulate matter and its specific chemical components from
887 cooking: A review, *Atmos. Environ.*, 71, 260-294,
888 doi:10.1016/j.atmosenv.2013.01.061,2013.

889 Agrios, K., Salazar, G. A., Zhang, Y. L., Uglietti, C., Battaglia, M., Luginbühl, M.,
890 Ciobanu, V. G., Vonwiller, M., and Szidat, S.: Online coupling of pure O₂
891 thermo-optical methods - ¹⁴C AMS for source apportionment of carbonaceous
892 aerosols study, *Nucl. Instrum. Meth. Phys. Res. B.*, 361, 288-293,
893 doi:10.1016/j.nimb.2015.06.008, 2015.

894 Aiken, A. C., DeCarlo, P. F., Kroll, J. H., Worsnop, D. R., Huffman, J. A., Docherty, K.
895 S., Ulbrich, I. M., Mohr, C., Kimmel, J. R., Sueper, D., Sun, Y., Zhang, Q.,
896 Trimborn, A., Northway, M., Ziemann, P. J., Canagaratna, M. R., Onasch, T. B.,
897 Alfarra, M. R., Prevot, A. S. H., Dommen, J., Duplissy, J., Metzger, A.,
898 Baltensperger, U., and Jimenez, J. L.: O/C and OM/OC ratios of primary,
899 secondary, and ambient organic aerosols with high-resolution time-of-flight
900 aerosol mass spectrometry, *Environ. Sci. Technol.*, 42, 4478-4485,
901 doi:10.1021/es703009q, 2008.

902 Alfarra, M. R., Prevot, A. S. H., Szidat, S., Sandradewi, J., Weimer, S., Lanz, V. A.,
903 Schreiber, D., Mohr, M., and Baltensperger, U.: Identification of the Mass
904 Spectral Signature of Organic Aerosols from Wood Burning Emissions, *Environ.*
905 *Sci. Technol.*, 41, 5770-5777, doi:10.1021/es062289b, 2007.

906 Beekmann, M., Prévôt, A. S. H., Drewnick, F., Sciare, J., Pandis, S. N., Denier van der
907 Gon, H. A. C., Crippa, M., Freutel, F., Poulain, L., Gherzi, V., Rodriguez, E.,
908 Beirle, S., Zotter, P., von der Weiden-Reinmüller, S.-L., Bressi, M., Fountoukis,
909 C., Petetin, H., Szidat, S., Schneider, J., Rosso, A., El Haddad, I., Megaritis, A.,
910 Zhang, Q. J., Michoud, V., Slowik, J. G., Moukhtar, S., Kolmonen, P., Stohl, A.,
911 Eckhardt, S., Borbon, A., Gros, V., Marchand, N., Jaffrezo, J. L.,
912 Schwarzenboeck, A., Colomb, A., Wiedensohler, A., Borrmann, S., Lawrence,
913 M., Baklanov, A., and Baltensperger, U.: In situ, satellite measurement and model
914 evidence on the dominant regional contribution to fine particulate matter levels in
915 the Paris megacity, *Atmos. Chem. Phys.*, 15, 9577-9591, doi:10.5194/acp-15-
916 9577-2015, 2015.

917 Bi, J., Huang, J., Hu, Z., Holben, B. N., and Guo, Z.: Investigating the aerosol optical and
918 radiative characteristics of heavy haze episodes in Beijing during January of 2013,
919 *J. Geophys. Res.*, 119, 9884-9900, doi:10.1002/2014JD021757, 2014.

920 Bond, T., and Bergstrom, R.: Light absorption by carbonaceous particles: An
921 investigative review, *Aerosol. Sci. Tech.*, 40, 27-67,
922 doi:10.1080/02786820500421521, 2006.

- 923 Canagaratna, M. R., Jayne, J. T., Jimenez, J. L., Allan, J. D., Alfarra, M. R., Zhang, Q.,
924 Onasch, T. B., Drewnick, F., Coe, H., Middlebrook, A., Delia, A., Williams, L.
925 R., Trimborn, A. M., Northway, M. J., DeCarlo, P. F., Kolb, C. E., Davidovits, P.,
926 and Worsnop, D. R.: Chemical and microphysical characterization of ambient
927 aerosols with the aerodyne aerosol mass spectrometer, *Mass Spectrom. Rev.*, 26,
928 185-222, doi:10.1002/mas.20115, 2007.
- 929 Canagaratna, M. R., Jimenez, J. L., Kroll, J. H., Chen, Q., Kessler, S. H., Massoli, P.,
930 Hildebrandt Ruiz, L., Fortner, E., Williams, L. R., Wilson, K. R., Surratt, J. D.,
931 Donahue, N. M., Jayne, J. T., and Worsnop, D. R.: Elemental ratio measurements
932 of organic compounds using aerosol mass spectrometry: Characterization,
933 improved calibration, and implications, *Atmos. Chem. Phys.*, 15, 253-272,
934 doi:10.5194/acp-15-253-2015, 2015.
- 935 Canonaco, F., Crippa, M., Slowik, J. G., Baltensperger, U., and Prévôt, A. S. H.: SoFi, an
936 IGOR-based interface for the efficient use of the generalized multilinear engine
937 (ME-2) for the source apportionment: ME-2 application to aerosol mass
938 spectrometer data, *Atmos. Meas. Tech.*, 6, 3649-3661, doi:10.5194/amt-6-3649-
939 2013, 2013.
- 940 Cao, C., Jiang, W., Wang, B., Fang, J., Lang, J., Tian, G., Jiang, J., and Zhu, T. F.:
941 Inhalable Microorganisms in Beijing's PM_{2.5} and PM₁₀ Pollutants during a
942 Severe Smog Event, *Environ. Sci. Technol.*, 48, 1499-1507,
943 doi:10.1021/es4048472, 2014.
- 944 Carlton, A. G., Bhave, P. V., Napelenok, S. L., Edney, E. O., Sarwar, G., Pinder, R. W.,
945 Pouliot, G. A., and Houyoux, M.: Model Representation of Secondary Organic
946 Aerosol in Cmaq4.7, *Environ. Sci. Technol.*, 44, 8553-8560,
947 doi:10.1021/es100636q, 2010.
- 948 Chan, C. K., and Yao, X.: Air pollution in mega cities in China, *Atmos. Environ.*, 42, 1-
949 42, doi:10.1016/j.atmosenv.2007.09.003, 2008.
- 950 Chen, Y., Zhao, C., Zhang, Q., Deng, Z., Huang, M., and Ma, X.: Aircraft study of
951 Mountain Chimney Effect of Beijing, China, *J. Geophys. Res.*, 114, D08306,
952 10.1029/2008JD010610, 2009.
- 953 Crippa, M., Canonaco, F., Lanz, V. A., Äijälä, M., Allan, J. D., Carbone, S., Capes, G.,
954 Ceburnis, D., Dall'Osto, M., Day, D. A., DeCarlo, P. F., Ehn, M., Eriksson, A.,
955 Freney, E., Hildebrandt Ruiz, L., Hillamo, R., Jimenez, J. L., Junninen, H.,
956 Kiendler-Scharr, A., Kortelainen, A. M., Kulmala, M., Laaksonen, A., Mensah,
957 A. A., Mohr, C., Nemitz, E., O'Dowd, C., Ovadnevaite, J., Pandis, S. N., Petäjä,
958 T., Poulain, L., Saarikoski, S., Sellegri, K., Swietlicki, E., Tiitta, P., Worsnop, D.
959 R., Baltensperger, U., and Prévôt, A. S. H.: Organic aerosol components derived
960 from 25 AMS data sets across Europe using a consistent ME-2 based source
961 apportionment approach, *Atmos. Chem. Phys.*, 14, 6159-6176, doi:10.5194/acp-
962 14-6159-2014, 2014.
- 963 Crippa, M., DeCarlo, P. F., Slowik, J. G., Mohr, C., Heringa, M. F., Chirico, R., Poulain,
964 L., Freutel, F., Sciare, J., Cozic, J., Di Marco, C. F., Elsasser, M., Nicolas, J. B.,

965 Marchand, N., Abidi, E., Wiedensohler, A., Drewnick, F., Schneider, J.,
966 Borrmann, S., Nemitz, E., Zimmermann, R., Jaffrezo, J. L., Prévôt, A. S. H., and
967 Baltensperger, U.: Wintertime aerosol chemical composition and source
968 apportionment of the organic fraction in the metropolitan area of paris, *Atmos.*
969 *Chem. Phys.*, 13, 961-981, doi:10.5194/acp-13-961-2013, 2013.

970 Dall'Osto, M., Ovadnevaite, J., Ceburnis, D., Martin, D., Healy, R. M., O'Connor, I. P.,
971 Kourtchev, I., Sodeau, J. R., Wenger, J. C., and O'Dowd, C.: Characterization of
972 urban aerosol in Cork city (Ireland) using aerosol mass spectrometry, *Atmos.*
973 *Chem. Phys.*, 13, 4997-5015, doi:10.5194/acp-13-4997-2013, 2013.

974 DeCarlo, P. F., Kimmel, J. R., Trimborn, A., Northway, M. J., Jayne, J. T., Aiken, A. C.,
975 Gonin, M., Fuhrer, K., Horvath, T., Docherty, K. S., Worsnop, D. R., and
976 Jimenez, J. L.: Field-Deployable, High-Resolution, Time-of-Flight Aerosol Mass
977 Spectrometer, *Anal. Chem.*, 78, 8281-8289, doi:10.1021/ac061249n, 2006.

978 Du, W., Sun, Y. L., Xu, Y. S., Jiang, Q., Wang, Q. Q., Yang, W., Wang, F., Bai, Z. P.,
979 Zhao, X. D., and Yang, Y. C.: Chemical characterization of submicron aerosol
980 and particle growth events at a national background site (3295 m a.s.l.) on the
981 Tibetan Plateau, *Atmos. Chem. Phys.*, 15, 10811-10824, doi:10.5194/acp-15-
982 10811-2015, 2015.

983 Dzepina, K., Arey, J., Marr, L. C., Worsnop, D. R., Salcedo, D., Zhang, Q., Onasch, T.
984 B., Molina, L. T., Molina, M. J., and Jimenez, J. L.: Detection of Particle-Phase
985 Polycyclic Aromatic Hydrocarbons in Mexico City Using an Aerosol Mass
986 Spectrometer, *Int. J. Mass Spectrom.*, 263, 152-170,
987 doi:10.1016/j.ijms.2007.01.010, 2007.

988 Elser, M., Huang, R. J., Wolf, R., Slowik, J. G., Wang, Q., Canonaco, F., Li, G., Bozzetti,
989 C., Daellenbach, K. R., Huang, Y., Zhang, R., Li, Z., Cao, J., Baltensperger, U.,
990 El-Haddad, I., and Prévôt, A. S. H.: New insights into pm2.5 chemical
991 composition and sources in two major cities in china during extreme haze events
992 using aerosol mass spectrometry, *Atmos. Chem. Phys.*, 16, 3207-3225,
993 doi:10.5194/acp-16-3207-2016, 2016.

994 Ge, X., Setyan, A., Sun, Y., and Zhang, Q.: Primary and secondary organic aerosols in
995 Fresno, California during wintertime: Results from high resolution aerosol mass
996 spectrometry, *J. Geophys. Res.*, 117, D19301, doi:10.1029/2012jd018026, 2012.

997 Hayes, P. L., Ortega, A. M., Cubison, M. J., Froyd, K. D., Zhao, Y., Cliff, S. S., Hu, W.
998 W., Toohey, D. W., Flynn, J. H., Lefer, B. L., Grossberg, N., Alvarez, S.,
999 Rappenglück, B., Taylor, J. W., Allan, J. D., Holloway, J. S., Gilman, J. B.,
1000 Kuster, W. C., de Gouw, J. A., Massoli, P., Zhang, X., Liu, J., Weber, R. J.,
1001 Corrigan, A. L., Russell, L. M., Isaacman, G., Worton, D. R., Kreisberg, N. M.,
1002 Goldstein, A. H., Thalman, R., Waxman, E. M., Volkamer, R., Lin, Y. H., Surratt,
1003 J. D., Kleindienst, T. E., Offenberg, J. H., Dusanter, S., Griffith, S., Stevens, P. S.,
1004 Brioude, J., Angevine, W. M., and Jimenez, J. L.: Organic aerosol composition
1005 and sources in Pasadena, California during the 2010 CalNex campaign, *J.*
1006 *Geophys. Res.*, 118, 9233-9257, doi:10.1002/jgrd.50530, 2013.

- 1007 He, K., Yang, F., Ma, Y., Zhang, Q., Yao, X., Chan, C. K., Cadle, S., Chan, T., and
1008 Mulawa, P.: The characteristics of PM_{2.5} in Beijing, China, *Atmos. Environ.*, 35,
1009 4959-4970, doi:10.1016/s1352-2310(01)00301-6, 2001.
- 1010 He, L.-Y., Huang, X.-F., Xue, L., Hu, M., Lin, Y., Zheng, J., Zhang, R., and Zhang, Y.-
1011 H.: Submicron aerosol analysis and organic source apportionment in an urban
1012 atmosphere in Pearl River Delta of China using high-resolution aerosol mass
1013 spectrometry, *J. Geophys. Res.*, 116, D12304, doi:10.1029/2010jd014566, 2011.
- 1014 He, L. Y., Lin, Y., Huang, X. F., Guo, S., Xue, L., Su, Q., Hu, M., Luan, S. J., and Zhang,
1015 Y. H.: Characterization of high-resolution aerosol mass spectra of primary organic
1016 aerosol emissions from Chinese cooking and biomass burning, *Atmos. Chem.*
1017 *Phys.*, 10, 11535-11543, doi:10.5194/acp-10-11535-2010, 2010.
- 1018 Heald, C. L., Kroll, J. H., Jimenez, J. L., Docherty, K. S., DeCarlo, P. F., Aiken, A. C.,
1019 Chen, Q., Martin, S. T., Farmer, D. K., and Artaxo, P.: A Simplified Description
1020 of the Evolution of Organic Aerosol Composition in the Atmosphere, *Geophys.*
1021 *Res. Lett.*, 37, L08803, doi:10.1029/2010gl042737, 2010.
- 1022 Herndon, S. C., Onasch, T. B., Wood, E. C., Kroll, J. H., Canagaratna, M. R., Jayne, J.
1023 T., Zavala, M. A., Knighton, W. B., Mazzoleni, C., Dubey, M. K., Ulbrich, I. M.,
1024 Jimenez, J. L., Seila, R., de Gouw, J. A., de Foy, B., Fast, J., Molina, L. T., Kolb,
1025 C. E., and Worsnop, D. R.: Correlation of secondary organic aerosol with odd
1026 oxygen in Mexico City, *Geophys. Res. Lett.*, 35, L15804,
1027 doi:10.1029/2008GL034058, 2008.
- 1028 Hodzic, A., Kasibhatla, P. S., Jo, D. S., Cappa, C. D., Jimenez, J. L., Madronich, S., and
1029 Park, R. J.: Rethinking the Global Secondary Organic Aerosol (Soa) Budget:
1030 Stronger Production, Faster Removal, Shorter Lifetime, *Atmos. Chem. Phys.*, 16,
1031 7917-7941, doi:10.5194/acp-16-7917-2016, 2016.
- 1032 Hu, W. W., Hu, M., Yuan, B., Jimenez, J. L., Tang, Q., Peng, J. F., Hu, W., Shao, M.,
1033 Wang, M., Zeng, L. M., Wu, Y. S., Gong, Z. H., Huang, X. F., and He, L. Y.:
1034 Insights on organic aerosol aging and the influence of coal combustion at a
1035 regional receptor site of central eastern China, *Atmos. Chem. Phys.*, 13, 10095-
1036 10112, doi:10.5194/acp-13-10095-2013, 2013.
- 1037 Hu, W., Hu, M., Hu, W., Jimenez, J. L., Yuan, B., Chen, W., Wang, M., Wu, Y., Chen,
1038 C., Wang, Z., Peng, J., Zeng, L., and Shao, M.: Chemical Composition, Sources,
1039 and Aging Process of Submicron Aerosols in Beijing: Contrast between Summer
1040 and Winter, *J. Geophys. Res.*, 121, 2015JD024020, doi: 10.1002/2015JD024020,
1041 2016.
- 1042 Huang, R.-J., Zhang, Y., Bozzetti, C., Ho, K.-F., Cao, J.-J., Han, Y., Daellenbach, K. R.,
1043 Slowik, J. G., Platt, S. M., Canonaco, F., Zotter, P., Wolf, R., Pieber, S. M.,
1044 Bruns, E. A., Crippa, M., Ciarelli, G., Piazzalunga, A., Schwikowski, M.,
1045 Abbazade, G., Schnelle-Kreis, J., Zimmermann, R., An, Z., Szidat, S.,
1046 Baltensperger, U., Haddad, I. E., and Prevot, A. S. H.: High secondary aerosol
1047 contribution to particulate pollution during haze events in China, *Nature*, 514,
1048 218-222, doi:10.1038/nature13774, 2014

- 1049 Huang, X.-F., Xue, L., Tian, X.-D., Shao, W.-W., Sun, T.-L., Gong, Z.-H., Ju, W.-W.,
 1050 Jiang, B., Hu, M., and He, L.-Y.: Highly time-resolved carbonaceous aerosol
 1051 characterization in Yangtze River Delta of China: Composition, mixing state and
 1052 secondary formation, *Atmos. Environ.*, **64**, 200-207,
 1053 doi:10.1016/j.atmosenv.2012.09.059, 2013.
- 1054 Huang, X. F., He, L. Y., Hu, M., Canagaratna, M. R., Kroll, J. H., Ng, N. L., Zhang, Y.
 1055 H., Lin, Y., Xue, L., Sun, T. L., Liu, X. G., Shao, M., Jayne, J. T., and Worsnop,
 1056 D. R.: Characterization of submicron aerosols at a rural site in Pearl River Delta
 1057 of China using an Aerodyne High-Resolution Aerosol Mass Spectrometer, *Atmos.*
 1058 *Chem. Phys.*, **11**, 1865-1877, doi:10.5194/acp-11-1865-2011, 2011.
- 1059 Ianniello, A., Spataro, F., Esposito, G., Allegrini, I., Hu, M., and Zhu, T.: Chemical
 1060 characteristics of inorganic ammonium salts in PM_{2.5} in the atmosphere of
 1061 Beijing (China), *Atmos. Chem. Phys.*, **11**, 10803-10822, doi:10.5194/acp-11-
 1062 10803-2011, 2011.
- 1063 Jayne, J. T., Leard, D. C., Zhang, X., Davidovits, P., Smith, K. A., Kolb, C. E., and
 1064 Worsnop, D. R.: Development of an Aerosol Mass Spectrometer for Size and
 1065 Composition Analysis of Submicron Particles, *Aerosol. Sci. Tech.*, **33**, 49 - 70,
 1066 doi:10.1080/027868200410840, 2000.
- 1067 Jimenez, J. L., Canagaratna, M. R., Donahue, N. M., Prevot, A. S. H., Zhang, Q., Kroll, J.
 1068 H., DeCarlo, P. F., Allan, J. D., Coe, H., Ng, N. L., Aiken, A. C., Docherty, K. S.,
 1069 Ulbrich, I. M., Grieshop, A. P., Robinson, A. L., Duplissy, J., Smith, J. D.,
 1070 Wilson, K. R., Lanz, V. A., Hueglin, C., Sun, Y. L., Tian, J., Laaksonen, A.,
 1071 Raatikainen, T., Rautiainen, J., Vaattovaara, P., Ehn, M., Kulmala, M.,
 1072 Tomlinson, J. M., Collins, D. R., Cubison, M. J., E., Dunlea, J., Huffman, J. A.,
 1073 Onasch, T. B., Alfarra, M. R., Williams, P. I., Bower, K., Kondo, Y., Schneider,
 1074 J., Drewnick, F., Borrmann, S., Weimer, S., Demerjian, K., Salcedo, D., Cottrell,
 1075 L., Griffin, R., Takami, A., Miyoshi, T., Hatakeyama, S., Shimono, A., Sun, J. Y.,
 1076 Zhang, Y. M., Dzepina, K., Kimmel, J. R., Sueper, D., Jayne, J. T., Herndon, S.
 1077 C., Trimborn, A. M., Williams, L. R., Wood, E. C., Middlebrook, A. M., Kolb, C.
 1078 E., Baltensperger, U., and Worsnop, D. R.: Evolution of organic aerosols in the
 1079 atmosphere, *Science*, **326**, 1525-1529, doi:10.1126/science.1180353, 2009.
- 1080 Liu, Z., Wang, Y., Vrekoussis, M., Richter, A., Wittrock, F., Burrows, J. P., Shao, M.,
 1081 Chang, C.-C., Liu, S.-C., Wang, H., and Chen, C.: Exploring the missing source
 1082 of glyoxal (CHOCHO) over China, *Geophys. Res. Lett.*, **39**, L10812,
 1083 doi:10.1029/2012GL051645, 2012.
- 1084 Minguillón, M. C., Perron, N., Querol, X., Szidat, S., Fahrni, S. M., Alastuey, A.,
 1085 Jimenez, J. L., Mohr, C., Ortega, A. M., Day, D. A., Lanz, V. A., Wacker, L.,
 1086 Reche, C., Cusack, M., Amato, F., Kiss, G., Hoffer, A., Decesari, S., Moretti, F.,
 1087 Hillamo, R., Teinilä, K., Seco, R., Peñuelas, J., Metzger, A., Schallhart, S.,
 1088 Müller, M., Hansel, A., Burkhardt, J. F., Baltensperger, U., and Prévôt, A. S. H.:
 1089 Fossil versus contemporary sources of fine elemental and organic carbonaceous
 1090 particulate matter during the DAURE campaign in Northeast Spain, *Atmos.*
 1091 *Chem. Phys.*, **11**, 12067-12084, doi:10.5194/acp-11-12067-2011, 2011.

- 1092 Mohr, C., DeCarlo, P. F., Heringa, M. F., Chirico, R., Slowik, J. G., Richter, R., Reche,
1093 C., Alastuey, A., Querol, X., Seco, R., Penuelas, J., Jimenez, J. L., Crippa, M.,
1094 Zimmermann, R., Baltensperger, U., and Prevot, A. S. H.: Identification and
1095 quantification of organic aerosol from cooking and other sources in Barcelona
1096 using aerosol mass spectrometer data, *Atmos. Chem. Phys.*, 12, 1649-1665,
1097 doi:10.5194/acp-12-1649-2012, 2012.
- 1098 Ng, N. L., Canagaratna, M. R., Zhang, Q., Jimenez, J. L., Tian, J., Ulbrich, I. M., Kroll, J.
1099 H., Docherty, K. S., Chhabra, P. S., Bahreini, R., Murphy, S. M., Seinfeld, J. H.,
1100 Hildebrandt, L., Donahue, N. M., DeCarlo, P. F., Lanz, V. A., Prévôt, A. S. H.,
1101 Dinar, E., Rudich, Y., and Worsnop, D. R.: Organic aerosol components observed
1102 in Northern Hemispheric datasets from Aerosol Mass Spectrometry, *Atmos.*
1103 *Chem. Phys.*, 10, 4625-4641, doi:10.5194/acp-10-4625-2010, 2010.
- 1104 Okuda, T., Naoi, D., Tenmoku, M., Tanaka, S., He, K., Ma, Y., Yang, F., Lei, Y., Jia, Y.,
1105 and Zhang, D.: Polycyclic Aromatic Hydrocarbons (Pahs) in the Aerosol in
1106 Beijing, China, Measured by Aminopropylsilane Chemically-Bonded Stationary-
1107 Phase Column Chromatography and Hplc/Fluorescence Detection, *Chemosphere*,
1108 65, 427-435, doi:10.1016/j.chemosphere.2006.01.064, 2006.
- 1109 Ortega, A. M., Day, D. A., Cubison, M. J., Brune, W. H., Bon, D., de Gouw, J. A., and
1110 Jimenez, J. L., Secondary organic aerosol formation and primary organic aerosol
1111 oxidation from biomass-burning smoke in a flow reactor during FLAME-3,
1112 *Atmos. Chem. Phys.*, 13(22), 11551-11571, doi:10.5194/acp-13-11551-2013,
1113 2013.
- 1114 Paatero, P., and Tapper, U.: Positive matrix factorization: A non-negative factor model
1115 with optimal utilization of error estimates of data values, *Environmetrics*, 5,
1116 doi:111-126, 10.1002/env.3170050203, 1994.
- 1117 Pusede, S. E., VandenBoer, T. C., Murphy, J. G., Markovic, M. Z., Young, C. J., Veres,
1118 P. R., Roberts, J. M., Washenfelder, R. A., Brown, S. S., Ren, X., Tsai, C., Stutz,
1119 J., Brune, W. H., Browne, E. C., Wooldridge, P. J., Graham, A. R., Weber, R.,
1120 Goldstein, A. H., Dusanter, S., Griffith, S. M., Stevens, P. S., Lefer, B. L., and
1121 Cohen, R. C.: An Atmospheric Constraint on the No₂ Dependence of Daytime
1122 near-Surface Nitrous Acid (HONO), *Environ. Sci. Technol.*, 49, 12774-12781,
1123 doi:10.1021/acs.est.5b02511, 2015.
- 1124 Song, Y., Xie, S., Zhang, Y., Zeng, L., Salmon, L. G., and Zheng, M.: Source
1125 apportionment of PM_{2.5} in Beijing using principal component analysis/absolute
1126 principal component scores and UNMIX, *Sci. Total. Environ.*, 372, 278-286,
1127 doi:10.1016/j.scitotenv.2006.08.041, 2006.
- 1128 Sun, Y., Du, W., Fu, P., Wang, Q., Li, J., Ge, X., Zhang, Q., Zhu, C., Ren, L., Xu, W.,
1129 Zhao, J., Han, T., Worsnop, D. R., and Wang, Z.: Primary and secondary aerosols
1130 in Beijing in winter: sources, variations and processes, *Atmos. Chem. Phys.*, 16,
1131 8309-8329, doi:10.5194/acp-16-8309-2016, 2016.

- 1132 Sun, Y., Jiang, Q., Wang, Z., Fu, P., Li, J., Yang, T., and Yin, Y.: Investigation of the
1133 sources and evolution processes of severe haze pollution in Beijing in January
1134 2013, *J. Geophys. Res.*, 119, 2014JD021641, doi:10.1002/2014JD021641, 2014.
- 1135 Sun, Y., Zhuang, G., Tang, A., Wang, Y., and An, Z.: Chemical Characteristics of PM_{2.5}
1136 and PM₁₀ in Haze–Fog Episodes in Beijing, *Environ. Sci. Technol.*, 40, 3148-
1137 3155, doi:10.1021/es051533g, 2006.
- 1138 Sun, Y., Zhang, Q., Zheng, M., Ding, X., Edgerton, E. S., and Wang, X.: Characterization
1139 and source apportionment of water-soluble organic matter in atmospheric fine
1140 particles (pm_{2.5}) with high-resolution aerosol mass spectrometry and gc-ms,
1141 *Environ. Sci. and Technol.*, 45, 4854 - 4861, doi:10.1021/es200162h, 2011a.
- 1142 Sun, Y., Zhang, Q., Schwab, J. J., Demerjian, K. L., Chen, W. N., Bae, M. S., Hung, H.
1143 M., Hogrefe, O., Frank, B., Rattigan, O. V., and Lin, Y. C.: Characterization of
1144 the sources and processes of organic and inorganic aerosols in New York city
1145 with a high-resolution time-of-flight aerosol mass spectrometer, *Atmos. Chem.*
1146 *Phys.*, 11, 1581-1602, doi:10.5194/acp-11-1581-2011, 2011b.
- 1147 Sun, Y. L., Wang, Z., Fu, P., Jiang, Q., Yang, T., Li, J., and Ge, X.: The impact of
1148 relative humidity on aerosol composition and evolution processes during
1149 wintertime in Beijing, China, *Atmos. Environ.*, 77, 927-934,
1150 doi:10.1016/j.atmosenv.2013.06.019, 2013a.
- 1151 Sun, Y. L., Wang, Z. F., Fu, P. Q., Yang, T., Jiang, Q., Dong, H. B., Li, J., and Jia, J. J.:
1152 Aerosol composition, sources and processes during wintertime in Beijing, China,
1153 *Atmos. Chem. Phys.*, 13, 4577-4592, doi:10.5194/acp-13-4577-2013, 2013b.
- 1154 Szidat, S.; Salazar, G. A.; Vogel, E.; Battaglia, M.; Wacker, L.; Synal, H. A.; Türlér, A.:
1155 ¹⁴C analysis and sample preparation at the new Bern Laboratory for the Analysis
1156 of Radiocarbon with AMS (LARA). *Radiocarbon*, 56, 561-566,
1157 doi:10.2458/56.17457, 2014.
- 1158 Tang, X. Y., Tian, B. S., Chen, C. H., and Ren, Z. H.: A study of photochemical smog
1159 pollution and its control stratiges at Xi-Gu district of Lanzhou city, China
1160 *Environ. Sci.*, 5(2), 1-11, 1985. (in Chinese with abstract in English)
- 1161 Ulbrich, I. M., Canagaratna, M. R., Zhang, Q., Worsnop, D. R., and Jimenez, J. L.:
1162 Interpretation of organic components from Positive Matrix Factorization of
1163 aerosol mass spectrometric data, *Atmos. Chem. Phys.*, 9, 2891-2918,
1164 doi:10.5194/acp-9-2891-2009, 2009.
- 1165 Volkamer, R., Jimenez, J. L., San Martini, F., Dzepina, K., Zhang, Q., Salcedo, D.,
1166 Molina, L. T., Worsnop, D. R., and Molina, M. J.: Secondary organic aerosol
1167 formation from anthropogenic air pollution: Rapid and higher than expected,
1168 *Geophys. Res. Lett.*, 33, L17811, doi:10.1029/2006GL026899, 2006.
- 1169 Wang, X., Cotter, E., Iyer, K. N., Fang, J., Williams, B. J., and Biswas, P.: Relationship
1170 between pyrolysis products and organic aerosols formed during coal combustion,
1171 *P. Combust. Inst.*, 35, 2347-2354, doi:10.1016/j.proci.2014.07.073, 2015.

- 1172 Wang, Y., Ying, Q., Hu, J., and Zhang, H.: Spatial and temporal variations of six criteria
1173 air pollutants in 31 provincial capital cities in China during 2013–2014, *Environ.*
1174 *Int.*, 73, 413–422, doi:10.1016/j.envint.2014.08.016, 2014.
- 1175 Wiedensohler, A., Birmili, W., Nowak, A., Sonntag, A., Weinhold, K., Merkel, M.,
1176 Wehner, B., Tuch, T., Pfeifer, S., Fiebig, M., Fjåraa, A. M., Asmi, E., Sellegri, K.,
1177 Depuy, R., Venzac, H., Villani, P., Laj, P., Aalto, P., Ogren, J. A., Swietlicki, E.,
1178 Williams, P., Roldin, P., Quincey, P., Hüglin, C., Fierz-Schmidhauser, R., Gysel,
1179 M., Weingartner, E., Riccobono, F., Santos, S., Gruning, C., Faloon, K.,
1180 Beddows, D., Harrison, R., Monahan, C., Jennings, S. G., O'Dowd, C. D.,
1181 Marinoni, A., Horn, H. G., Keck, L., Jiang, J., Scheckman, J., McMurry, P. H.,
1182 Deng, Z., Zhao, C. S., Moerman, M., Henzing, B., de Leeuw, G., Löschau, G.,
1183 and Bastian, S.: Mobility particle size spectrometers: harmonization of technical
1184 standards and data structure to facilitate high quality long-term observations of
1185 atmospheric particle number size distributions, *Atmos. Meas. Tech.*, 5, 657–685,
1186 doi:10.5194/amt-5-657-2012, 2012.
- 1187 Wood, E. C., Canagaratna, M. R., Herndon, S. C., Onasch, T. B., Kolb, C. E., Worsnop,
1188 D. R., Kroll, J. H., Knighton, W. B., Seila, R., Zavala, M., Molina, L. T.,
1189 DeCarlo, P. F., Jimenez, J. L., Weinheimer, A. J., Knapp, D. J., Jobson, B. T.,
1190 Stutz, J., Kuster, W. C., and Williams, E. J.: Investigation of the correlation
1191 between odd oxygen and secondary organic aerosol in Mexico City and Houston,
1192 *Atmos. Chem. Phys.*, 10, 8947–8968, doi:10.5194/acp-10-8947-2010, 2010.
- 1193 Xu, J., Zhang, Q., Chen, M., Ge, X., Ren, J., and Qin, D.: Chemical composition, sources,
1194 and processes of urban aerosols during summertime in northwest China: insights
1195 from high-resolution aerosol mass spectrometry, *Atmos. Chem. Phys.*, 14, 12593–
1196 12611, doi:10.5194/acp-14-12593-2014, 2014.
- 1197 Young, C. J., Washenfelder, R. A., Roberts, J. M., Mielke, L. H., Osthoff, H. D., Tsai,
1198 C., Pikelnaya, O., Stutz, J., Veres, P. R., Cochran, A. K., VandenBoer, T.
1199 C., Flynn, J., Grossberg, N., Haman, C. L., Lefer, B., Stark, H., Graus, M.,
1200 de Grouw, J., Gilman, J. B., Kuster, W. C., and Brown, S. S.: Vertically
1201 resolved measurements of nighttime radical reservoirs in Los Angeles and their
1202 contribution to the urban radical budget, *Environ. Sci. Technol.*, 46, 10965–
1203 10973, doi:10.1021/es302206a, 2012.
- 1204 Young, D. E., Kim, H., Parworth, C., Zhou, S., Zhang, X., Cappa, C. D., Seco, R., Kim,
1205 S., and Zhang, Q.: Influences of emission sources and meteorology on aerosol
1206 chemistry in a polluted urban environment: results from DISCOVER-AQ
1207 California, *Atmos. Chem. Phys.*, 16, 5427–5451, 10.5194/acp-16-5427-2016,
1208 2016.
- 1209 Yu, L., Wang, G., Zhang, R., Zhang, L., Song, Y., Wu, B., Li, X., An, K., and Chu, J.:
1210 Characterization and Source Apportionment of PM_{2.5} in an Urban Environment
1211 in Beijing, *Aerosol Air Qual. Res.*, 13, 574–583, doi:10.4209/aaqr.2012.07.0192,
1212 2013.

- 1213 Zhang, J. K., Sun, Y., Liu, Z. R., Ji, D. S., Hu, B., Liu, Q., and Wang, Y. S.:
1214 Characterization of submicron aerosols during a month of serious pollution in
1215 Beijing, 2013, *Atmos. Chem. Phys.*, 14, 2887-2903, doi:10.5194/acp-14-2887-
1216 2014, 2014.
- 1217 Zhang, L., Chen, C., Li, S., and Zhang, F.: Air pollution and potential control schemes in
1218 Lanzhou, *Res. Environ. Sci.*, 13(4), 18-21, 2000.
- 1219 Zhang, Q., Canagaratna, M. R., Jayne, J. T., Worsnop, D. R., and Jimenez, J. L.: Time-
1220 and size-resolved chemical composition of submicron particles in Pittsburgh:
1221 Implications for aerosol sources and processes, *J. Geophys. Res.*, 110, D07s09,
1222 doi:10.1029/2004jd004649, 2005.
- 1223 Zhang, Q., Jimenez, J. L., Canagaratna, M. R., Ulbrich, I. M., Ng, N. L., Worsnop, D. R.,
1224 and Sun, Y.: Understanding atmospheric organic aerosols via factor analysis of
1225 aerosol mass spectrometry: a review, *Anal. Bioanal. Chem.*, 401, 3045-3067,
1226 doi:10.1007/s00216-011-5355-y, 2011a.
- 1227 Zhang, Q., and Li, H.: A study of the relationship between air pollutants and inversion in
1228 the ABL over the city of Lanzhou, *Adv. Atmos. Sci.*, 28(4), 879-886, doi:
1229 10.1007/s00376-010-0079-z, 2011b.
- 1230 Zhang, R., Jing, J., Tao, J., Hsu, S. C., Wang, G., Cao, J., Lee, C. S. L., Zhu, L., Chen, Z.,
1231 Zhao, Y., and Shen, Z.: Chemical characterization and source apportionment of
1232 PM_{2.5} in Beijing: seasonal perspective, *Atmos. Chem. Phys.*, 13, 7053-7074,
1233 doi:10.5194/acp-13-7053-2013, 2013.
- 1234 Zhang, Y., Schauer, J. J., Zhang, Y., Zeng, L., Wei, Y., Liu, Y., and Shao, M.:
1235 Characteristics of Particulate Carbon Emissions from Real-World Chinese Coal
1236 Combustion, *Environ. Sci. Technol.*, 42, 5068-5073, doi:10.1021/es7022576,
1237 2008.
- 1238 Zhang, Y. J., Tang, L. L., Wang, Z., Yu, H. X., Sun, Y. L., Liu, D., Qin, W., Canonaco,
1239 F., Prévôt, A. S. H., Zhang, H. L., and Zhou, H. C.: Insights into characteristics,
1240 sources, and evolution of submicron aerosols during harvest seasons in the
1241 Yangtze River delta region, China, *Atmos. Chem. Phys.*, 15, 1331-1349,
1242 doi:10.5194/acp-15-1331-2015, 2015a.
- 1243 Zhang, Y. L., Huang, R. J., El Haddad, I., Ho, K. F., Cao, J. J., Han, Y., Zotter, P.,
1244 Bozzetti, C., Daellenbach, K. R., Canonaco, F., Slowik, J. G., Salazar, G.,
1245 Schwikowski, M., Schnelle-Kreis, J., Abbaszade, G., Zimmermann, R.,
1246 Baltensperger, U., Prévôt, A. S. H., and Szidat, S.: Fossil vs. Non-fossil sources of
1247 fine carbonaceous aerosols in four Chinese cities during the extreme winter haze
1248 episode of 2013, *Atmos. Chem. Phys.*, 15, 1299-1312, 10.5194/acp-15-1299-
1249 2015, 2015b.
- 1250 Zhang, Y. L.; Perron, N.; Ciobanu, V. G.; Zotter, P.; Minguillón, M. C.; Wacker, L.;
1251 Prévôt, A. S. H.; Baltensperger, U.; Szidat, S.: On the isolation of OC and EC and
1252 the optimal strategy of radiocarbon-based source apportionment of carbonaceous

- 1253 aerosols. *Atmos. Chem. Phys.*, 12, 10841-10856, doi:10.5194/acp-12-10841-
1254 2012, 2012.
- 1255 Zhang, Z., Wang, X., Zhang, Y., Lü, S., Huang, Z., Huang, X., and Wang, Y.: Ambient
1256 air benzene at background sites in China's most developed coastal regions:
1257 Exposure levels, source implications and health risks, *Sci. Total. Environ.*, 511,
1258 792-800, doi:10.1016/j.scitotenv.2015.01.003, 2015c.
- 1259 Zhao, X. J., Zhao, P. S., Xu, J., Meng, W., Pu, W. W., Dong, F., He, D., and Shi, Q. F.:
1260 Analysis of a winter regional haze event and its formation mechanism in the
1261 North China Plain, *Atmos. Chem. Phys.*, 13, 5685-5696, doi:10.5194/acp-13-
1262 5685-2013, 2013.
- 1263 Zheng, G. J., Duan, F. K., Su, H., Ma, Y. L., Cheng, Y., Zheng, B., Zhang, Q., Huang, T.,
1264 Kimot, T., Chang, D., Poschl, U., Cheng, Y. F., and He, K. B.: Exploring the
1265 severe winter haze in Beijing: the impact of synoptic weather, regional transport
1266 and heterogeneous reactions. *Atmos. Chem. Phys.*, **15**(6), 2969-2983
1267 doi:10.5194/acp-15-2969-2015, 2015.
- 1268 Zheng, M., Salmon, L. G., Schauer, J. J., Zeng, L., Kiang, C. S., Zhang, Y., and Cass, G.
1269 R.: Seasonal trends in PM_{2.5} source contributions in Beijing, China, *Atmos.*
1270 *Environ.*, 39, 3967-3976, doi:10.1016/j.atmosenv.2005.03.036, 2005.
- 1271 Zotter, P., El-Haddad, I., Zhang, Y., Hayes, P. L., Zhang, X., Lin, Y.-H., Wacker, L.,
1272 Schnelle-Kreis, J., Abbaszade, G., Zimmermann, R., Surratt, J. D., Weber, R.,
1273 Jimenez, J. L., Szidat, S., Baltensperger, U., and Prévôt, A. S. H.: Diurnal cycle of
1274 fossil and nonfossil carbon using radiocarbon analyses during CalNex, *Journal of*
1275 *Geophysical Research: Atmospheres*, 119, 6818-6835,
1276 doi:10.1002/2013JD021114, 2014.

1277

1278 Table 1 Comparison of the composition of category ions and elemental composition of

1279 OA between winter 2013/2014 and summer 2012.

1280

Category Ions	Winter 2014	Summer 2012
$C_xH_y^+$	59%	56%
$C_xH_yO_1^+$	26%	27%
$C_xH_yO_2^+$	10%	11%
$C_xH_yN_p^+$	2%	3%
$C_xH_yN_pO_z^+$	0	1%
$H_yO_1^+$	2%	2%
Elemental composition		
C	67%	59%
H	9%	7%
O	23%	26%
N	1%	1%

1281

1282 Table 2 Coefficient of determination (R^2) between time series of OA factors and other

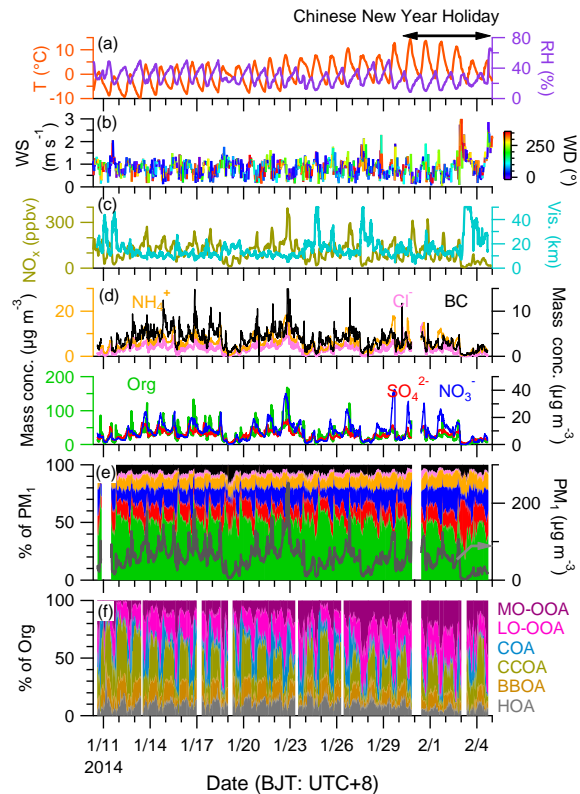
1283 aerosol species.

R^2	HOA	BBOA	COA	CCOA	LO-OOA	MO-OOA	POA*	SOA*
BC	0.64	0.67	0.24	0.59	0.20	0.06	0.64	0.16
PAH	0.40	0.64	0.25	0.58	0.02	0.00	0.61	0.01
Sulphate	0.35	0.24	0.17	0.22	0.71	0.34	0.32	0.64
Nitrate	0.19	0.04	0.15	0.02	0.74	0.71	0.16	0.85
Chloride	0.52	0.52	0.19	0.49	0.45	0.13	0.50	0.35
Sulphate + Nitrate	0.27	0.10	0.18	0.07	0.81	0.62	0.23	0.85
Sulphate + Nitrate + Chloride	0.35	0.18	0.19	0.15	0.77	0.52	0.32	0.77

1284

* POA = HOA + BBOA + COA + CCOA, SOA = LO-OOA + MO-OOA

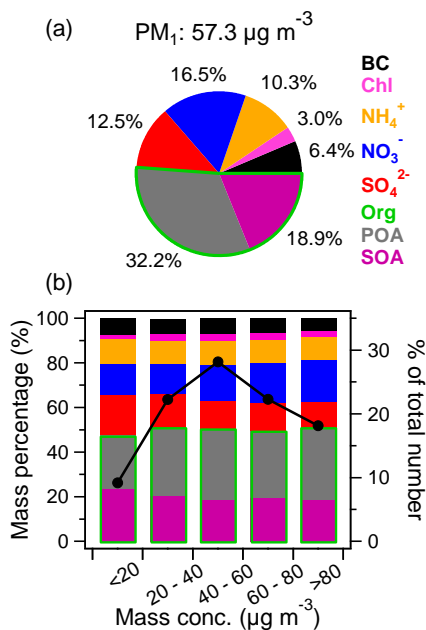
1285



1286
 1287
 1288
 1289
 1290
 1291
 1292
 1293

Fig. 1 Summary of meteorological and aerosol species data. (a) air temperature (T) and relative humidity (RH), (b) wind speed (WS) colored by wind direction (WD), (c) NO_x and visibility, (d) mass concentration of PM₁ species (BC is from aethalometer measurement), and (e) the mass contribution of PM₁ species (BC is from aethalometer measurement), and (f) the mass contribution of organic components to organic aerosol. Note that BC is from aethalometer measurement.

1294

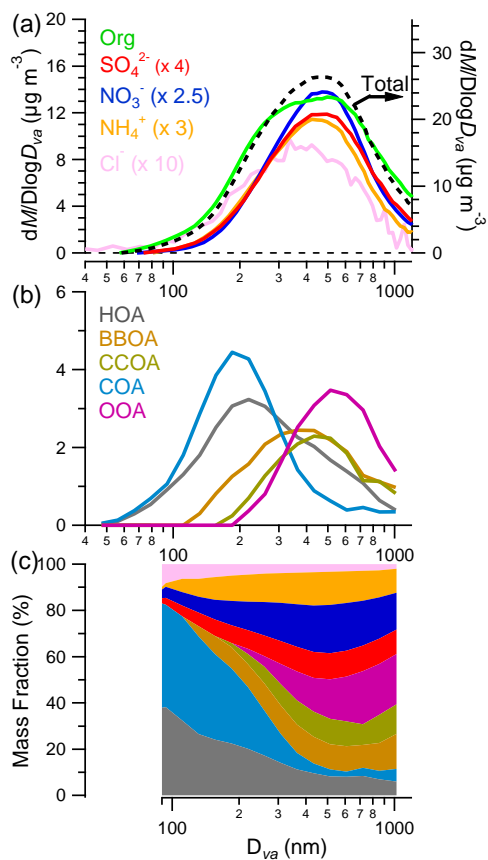


1295

1296

1297 Fig. 2 The average mass contribution of PM_1 (= NR- PM_1 + BC) species (a) during the
1298 whole sampling period and (b) as a function of the PM_1 mass concentration ($\mu g m^{-3}$) bins
1299 (left). The right axis in (b) shows the percentage of the data number in each bin to the
1300 total data number. The organics were decomposed into primary organic aerosol (POA)
1301 and secondary organic aerosol (SOA) using PMF (section 3.4).

1302

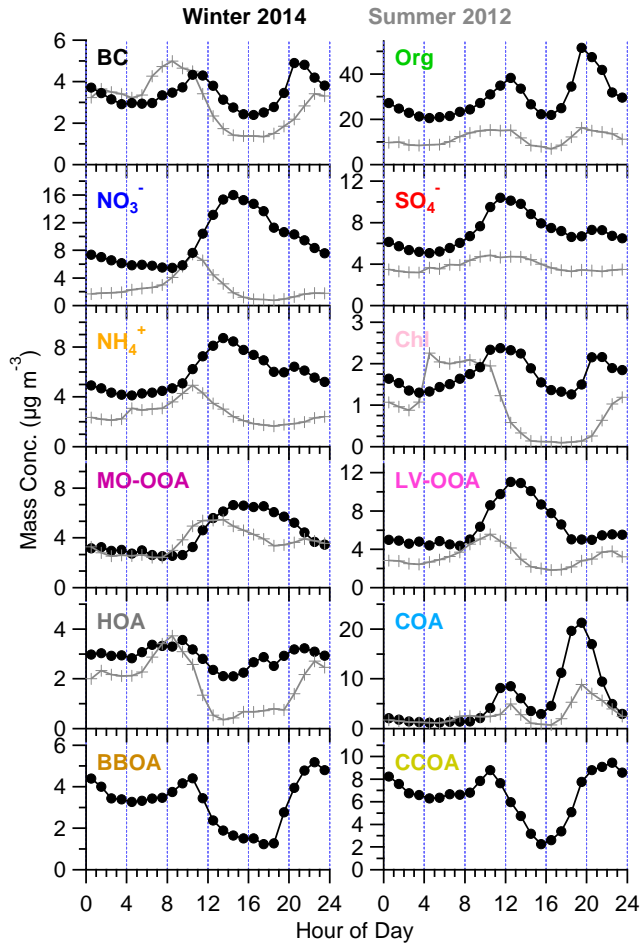


1303

1304 Fig. 3 The size distributions of (a) NR-PM₁ species, (b) organic components, and mass

1305 contribution of all species to NR-PM₁.

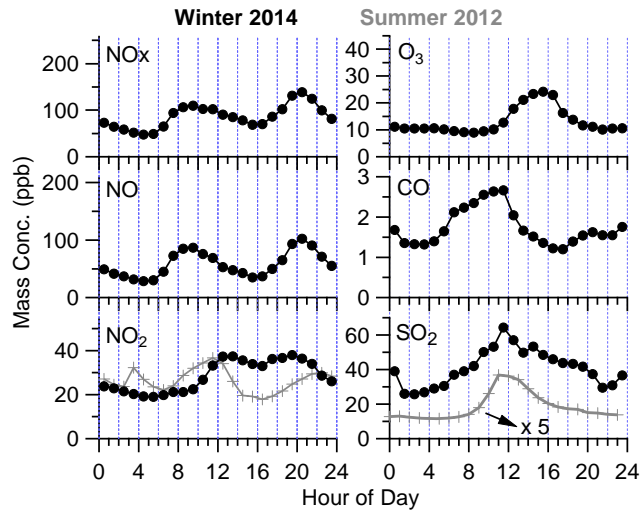
1306



1307

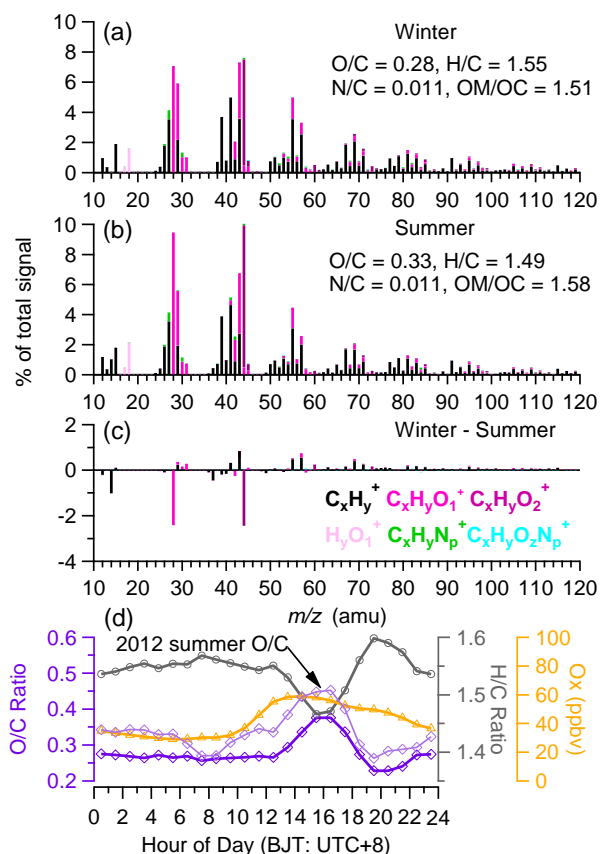
1308 Fig. 4 The diurnal variation of PM₁ species during winter 2013/2014 and summer 2012.

1309

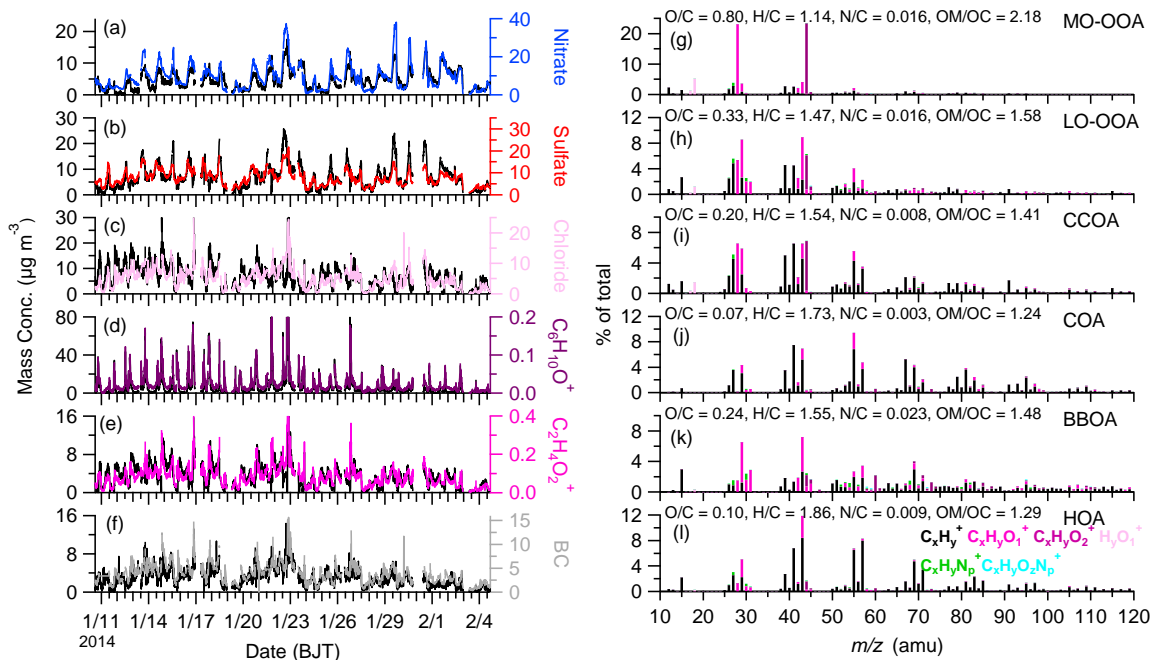


1310

1311 Fig. 5 The diurnal variations of gas species downloaded from MEP-China station during
 1312 winter 2013/2014 and summer 2012.
 1313



1314
 1315 Fig. 6 The average HR-MS and elemental ratios of organics for (a) this study, (b) summer
 1316 2012, (c) the HR-MS difference between this study and summer 2012, and (d) the
 1317 diurnal variations of elemental ratios and odd oxygen ($O_x = NO_2 + O_3$).
 1318

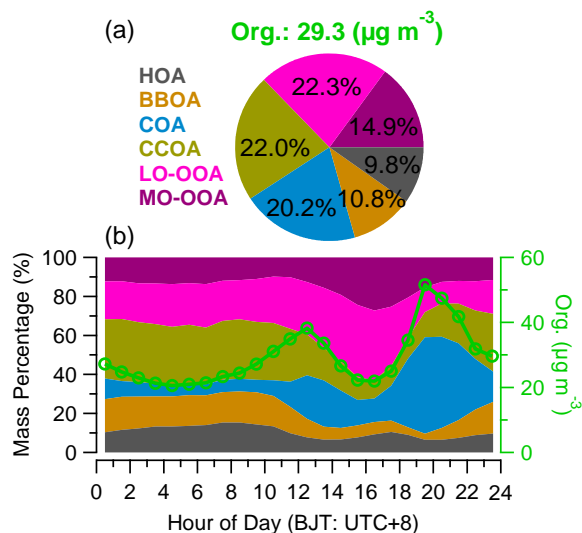


1319

1320 Fig. 7 The PMF results of time series (a – f) and HR-MS (g – l) for each component. The

1321 temporal variations of different tracers are also present for supporting each component.

1322



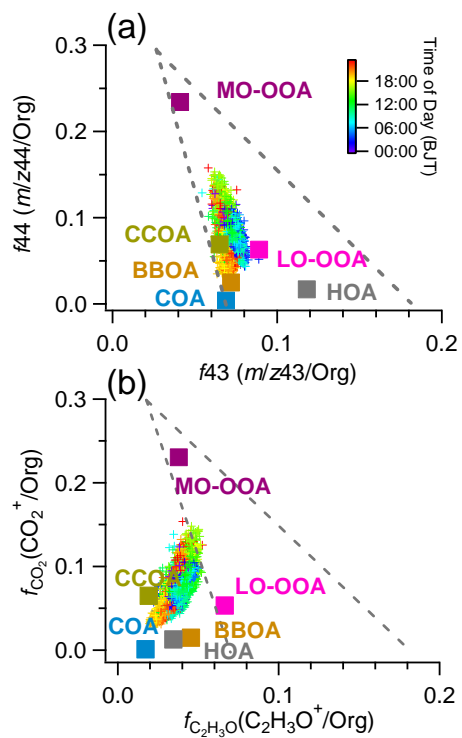
1323

1324 Fig. 8 (a) The average mass concentration of organics and mass contributions of organic

1325 components to organics, and (b) the diurnal variations of organic components and

1326 organics.

1327



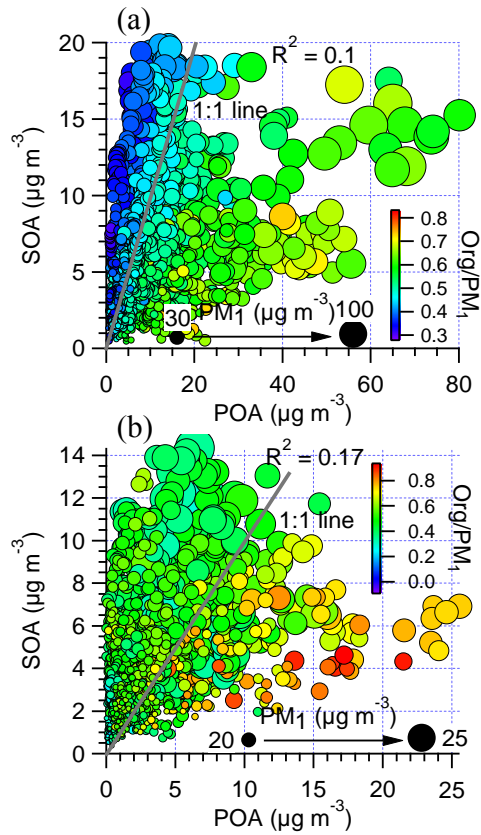
1328

1329 Fig. 9 Scatterplots of (a) f_{44} vs. f_{43} and (b) $f_{\text{CO}_2^+}$ vs. $f_{\text{C}_2\text{H}_3\text{O}^+}$. The cross dots correspond
 1330 to measured OA data points are colored by time of the day. The corresponding values of
 1331 the six OA factors identified in this study are also shown.

1332

1333

1334



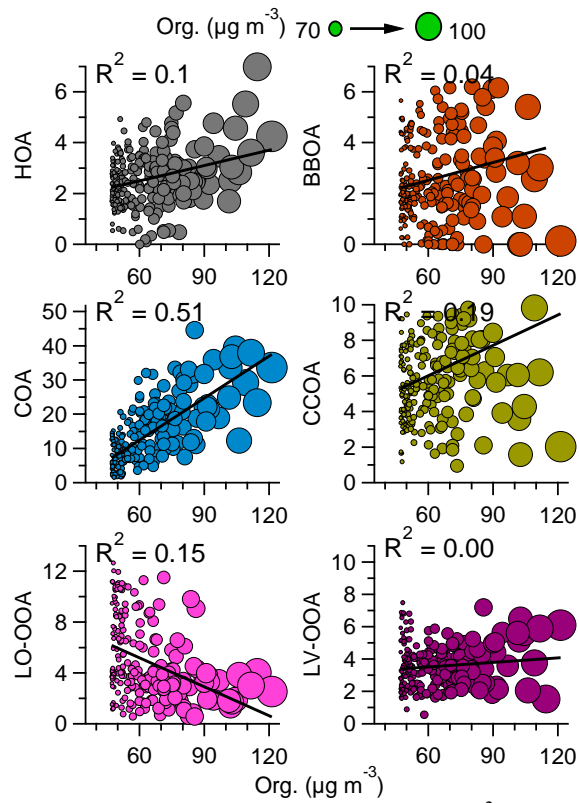
1335

1336 Fig. 10 The scatter plot of SOA and POA colored by the ratio of Org/PM_{10} and sized by

1337

the mass concentration of PM_{10} for (a) winter 2013/2014 and (b) summer 2012.

1338

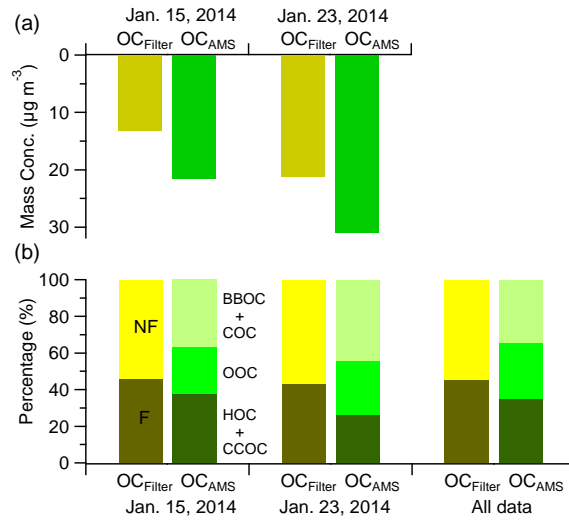


1339

1340 Fig. 11 The scatter plots of each organic component ($\mu\text{g m}^{-3}$) versus organics during haze

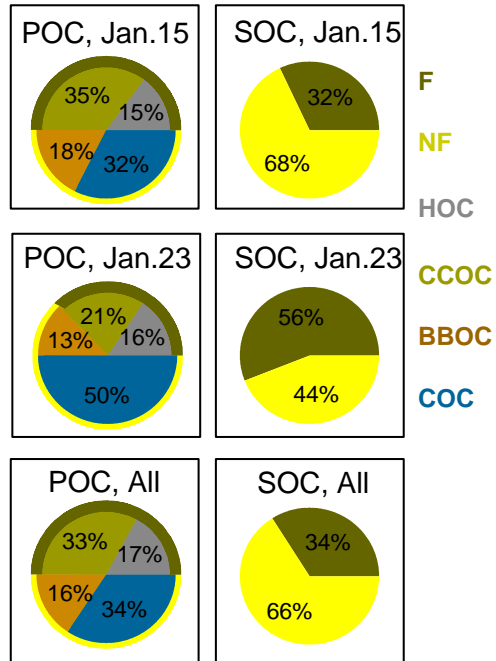
1341 periods (definite as organics $> 43 \mu\text{g m}^{-3}$ ($\text{Org_avg} + 1\sigma$))

1342



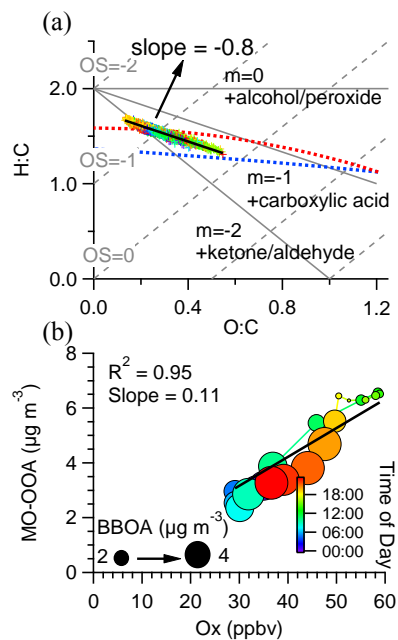
1343
 1344
 1345
 1346
 1347

Fig. 12 The comparisons of (a) OC concentration measured by filter sample ($\text{OC}_{\text{Filter}}$) and AMS (OC_{AMS}) on Jan. 15 and 23, 2014 and (b) the non-fossil (NF) and fossil (F) carbon fraction measured by ^{14}C and OC components in AMS.



1348
 1349
 1350
 1351

Fig. 13 The non-fossil (NF) and fossil (F) carbon fraction in POC and SOC during Jan. 15, Jan. 23 and all data of AMS.



1352

1353 Fig. 14 (a) Van Krevelen diagram for OA and (b) scatter plot of MO-OOA vs. O_x (the
 1354 sum of O_3 and NO_2) with linear fit and colored by time of day.

1355

1356